

SHORT REPORTS

Alternative splicing of *METTL3* explains apparently METTL3-independent m⁶A modifications in mRNAHui Xian Poh, Aashiq H. Mirza, Brian F. Pickering, Samie R. Jaffrey *

Department of Pharmacology, Weill Cornell Medicine, Cornell University, New York, New York, United States of America

* srj2003@med.cornell.edu OPEN ACCESS

Citation: Poh HX, Mirza AH, Pickering BF, Jaffrey SR (2022) Alternative splicing of *METTL3* explains apparently METTL3-independent m⁶A modifications in mRNA. *PLoS Biol* 20(7): e3001683. <https://doi.org/10.1371/journal.pbio.3001683>

Academic Editor: Wendy V Gilbert, Yale University, UNITED STATES

Received: December 1, 2021

Accepted: May 19, 2022

Published: July 19, 2022

Copyright: © 2022 Poh et al. This is an open access article distributed under the terms of the [Creative Commons Attribution License](https://creativecommons.org/licenses/by/4.0/), which permits unrestricted use, distribution, and reproduction in any medium, provided the original author and source are credited.

Data Availability Statement: Data from the 21Q4 DepMap study is available from the Broad Institute's DepMap Consortium and is accessible at <https://depmap.org/portal/download/>. All other relevant data are within the paper and its [Supporting information files](#).

Funding: This work was supported by National Institutes of Health (NIH, <https://www.nih.gov/>) grants R35NS111631, R01CA186702, and S100D030335 to S.R.J and F32CA22104 to B.F.P., and by Agency for Science, Technology and

Abstract

N⁶-methyladenosine (m⁶A) is a highly prevalent mRNA modification that promotes degradation of transcripts encoding proteins that have roles in cell development, differentiation, and other pathways. METTL3 is the major methyltransferase that catalyzes the formation of m⁶A in mRNA. As 30% to 80% of m⁶A can remain in mRNA after METTL3 depletion by CRISPR/Cas9-based methods, other enzymes are thought to catalyze a sizable fraction of m⁶A. Here, we reexamined the source of m⁶A in the mRNA transcriptome. We characterized mouse embryonic stem cell lines that continue to have m⁶A in their mRNA after *Mettl3* knockout. We show that these cells express alternatively spliced *Mettl3* transcript isoforms that bypass the CRISPR/Cas9 mutations and produce functionally active methyltransferases. We similarly show that other reported *METTL3* knockout cell lines express altered METTL3 proteins. We find that gene dependency datasets show that most cell lines fail to proliferate after *METTL3* deletion, suggesting that reported *METTL3* knockout cell lines express altered METTL3 proteins rather than have full knockout. Finally, we reassessed METTL3's role in synthesizing m⁶A using an exon 4 deletion of *Mettl3* and found that METTL3 is responsible for >95% of m⁶A in mRNA. Overall, these studies suggest that METTL3 is responsible for the vast majority of m⁶A in the transcriptome, and that remaining m⁶A in putative *METTL3* knockout cell lines is due to the expression of altered but functional METTL3 isoforms.

Introduction

N⁶-methyladenosine (m⁶A) is the most abundant internal mRNA modification [1–3], and its presence in mRNA is critical for cellular differentiation [4–6], cancer progression [7–9], and other cellular processes [10–14]. m⁶A in mRNA can regulate mRNA fates (reviewed by [15–17]), particularly by promoting mRNA degradation.

The first enzyme shown to catalyze m⁶A formation was METTL3 [18], which forms a heterodimer complex with METTL14 [19–21]. METTL3 contains the catalytic component. METTL14 was initially believed to have catalytic ability [21], but METTL14 is now known to

Research (A* STAR, <https://www.a-star.edu.sg/>) National Science Scholarship to H.X.P. The funders had no role in study design, data collection and analysis, decision to publish, or preparation of the manuscript.

Competing interests: I have read the journal's policy and the authors of this manuscript have the following competing interests: S.R.J. is scientific founder of, is advisor to, and owns equity in Gotham Therapeutics and 858 Therapeutics.

Abbreviations: DepMap, Dependency Map Project; FBS, fetal bovine serum; m⁶A, N⁶-methyladenosine; MEF, mouse embryonic fibroblast; mESC, mouse embryonic stem cell; ORF, open reading frame; PBS, phosphate buffered saline; RACE, rapid amplification of cDNA ends; WT, wild-type; ZFD, zinc finger domain.

be catalytically inactive [19,20]. Instead, METTL14 binds and positions RNA for methylation [19,20]. The METTL3-METTL14 complex is a component of a larger multiprotein “m⁶A writer complex” that mediates co-transcriptional mRNA methylation [17,22].

Although METTL3 is often described as the major m⁶A-forming enzyme in cells, the amount of m⁶A thought to be formed by METTL3 varies widely in different studies. The first study to knockout *Mettl3* showed that approximately 40% of m⁶A remained after *Mettl3* knockout in mouse embryonic stem cells (mESCs) [4]. The authors suggested that METTL14 may account for this 40% of m⁶A, based on the previous understanding that METTL14 was catalytic. However, a different group shortly thereafter reported that deletion of either *Mettl3* or *Mettl14* in mESCs leads to a loss of approximately 99% of m⁶A in mRNA [5]. These contradictory results have led to uncertainty about how much m⁶A in mRNA derives from METTL3.

METTL3 has been knocked out in other cell lines and tissues. These results have shown that 30% to 80% of m⁶A can remain after *METTL3* knockout [23–33]. In U2OS osteosarcoma cells, approximately 60% of m⁶A remained after CRISPR-mediated knockout of *METTL3* [23,24]. In HEK293T human embryonic kidney cells, approximately 50% of m⁶A remained after CRISPR-mediated knockout of *METTL3* [25]. After Cre-conditional genomic deletion of *Mettl3* in mouse CD4+ T cells, 28% of m⁶A remained [30]. Since a nonnegligible amount of m⁶A persists after *METTL3* knockout, it has been speculated that other methyltransferases may have a major role in forming m⁶A in mRNA [4,31,33–35].

Here, we address the source of m⁶A in mRNA in reported *METTL3* knockout cells. We examined two different *Mettl3* knockout mESC lines, which both report loss of METTL3, but showed vastly different levels of residual m⁶A in mRNA. We show that *Mettl3* mutagenesis by CRISPR approaches can create alternatively spliced isoforms of *Mettl3*, resulting in an altered but catalytically active METTL3 protein. Thus, the residual m⁶A can be ascribed to a hypomorphic *METTL3* allele. We further show that other published *METTL3* mutant cell lines, which were intended to delete *METTL3*, retain m⁶A and express alternative METTL3 proteins. Furthermore, we show that *METTL3* is an essential gene in most cell lines, and thus, *METTL3* knockout cell lines that remain viable are likely to have generated alternatively spliced functional METTL3 proteins that bypass the CRISPR mutations. Lastly, we show that when a large deletion is created in *METTL3*, essentially all m⁶A is depleted in a fibroblast cell line. Overall, these studies argue that METTL3 is responsible for most m⁶A in mRNA, and that residual m⁶A after *METTL3* depletion usually reflects the generation of hypomorphic *METTL3* alleles and therefore incomplete *METTL3* knockout.

Results

Two mESC lines exhibit different levels of m⁶A after *Mettl3* knockout

To understand how much m⁶A in mRNA is catalyzed by METTL3, we examined 2 previously reported *Mettl3* knockout mESC lines. Two groups independently knocked out *Mettl3* in mESCs and reported markedly different levels of residual m⁶A levels in mRNA [4,5]. The first *Mettl3* knockout mESC line was described by Batista and colleagues from Howard Chang's group, and used a CRISPR/Cas9 approach [4]. The guide RNAs were designed to introduce deletions in exon 2 of *Mettl3* and create premature termination codons [4]. The resulting mESC line, designated “exon2 *Mettl3* KO mESCs,” was found to have 40% residual m⁶A in mRNA. These authors understandably attributed the remaining m⁶A to METTL14 since, at that time, METTL14 was incorrectly shown to be a functional methyltransferase [21]. The second mESC line was described by Geula and colleagues from Jacob Hanna's group [5]. This group used *loxP* sites surrounding exon 4 in *Mettl3* to delete the exon encoding the zinc finger domain (ZFD), an RNA recognition domain required for METTL3 methyltransferase activity

[19,36]. This *Mettl3* knockout mESC line, designated “exon4 *Mettl3* KO mESCs,” exhibited <1% remaining m⁶A in mRNA. It is unclear why the exon2 *Mettl3* KO mESCs have high m⁶A levels when the exon4 *Mettl3* KO mESCs, which in principle should be the same, have virtually no remaining m⁶A.

We first reconfirmed the levels of m⁶A in these two cell lines. The m⁶A levels in the two *Mettl3* knockout mESC lines were originally measured via different methods, which may have led to these contradictory results. Thin-layer chromatography was used by Batista and colleagues [4], while mass spectrometry was used by Geula and colleagues [5]. We measured m⁶A in the mESC lines using mass spectrometry [37]. Our mass spectrometry measurements were consistent with the results originally reported by the two groups. In the two exon2 *Mettl3* KO mESC lines, designated exon2 *Mettl3* KO mESC-a and exon2 *Mettl3* KO mESC-b, we saw 40.2% and 55.6% residual m⁶A (Fig 1A), comparable to approximately 40% originally reported by this group [4]. However, the exon4 *Mettl3* KO mESCs had only 1.45% residual m⁶A (Fig 1A), corroborating the 0.5% remaining m⁶A originally reported by this group [5].

The near-complete loss of m⁶A in the exon4 *Mettl3* KO mESCs suggests that METTL3 is the major m⁶A writer in this mESC line. On the other hand, the exon2 *Mettl3* KO mESCs still retain m⁶A despite *Mettl3* depletion. Although it is possible that these mESCs use an alternate enzyme for m⁶A biosynthesis, we suspected that *Mettl3* was not completely knocked out in these cell lines.

***Mettl3* knockout mESCs that retain m⁶A express alternative *Mettl3* isoforms**

We next wanted to confirm that *Mettl3* was knocked out in the exon2 *Mettl3* KO mESCs. Previously, a western blot was used to determine the loss of METTL3 protein [4]. To first confirm that the METTL3 protein is indeed absent, we performed a western blot using a METTL3 polyclonal antibody raised against amino acids 229–580 of METTL3, which correspond to amino acids encoded by exons 3–11. Full-length METTL3 (approximately 75 kDa) was identified in the wild-type (WT) mESCs, and was lost in both *Mettl3* KO cell lines (Fig 1B). However, we observed new bands in the anti-METTL3 immunoblot in the knockout cell lines. The new proteins were approximately 50 kDa in exon2 *Mettl3* KO mESC-a and approximately 55 kDa in exon2 *Mettl3* KO mESC-b (Fig 1B). While nonspecific background bands are visible in all 3 cell lines, these particular proteins were not visible in the WT cell line, suggesting they are unique to the knockout cell lines and not just background. These proteins were also not visible in the exon4 *Mettl3* KO cell lines (Figs 1B and S1B).

To confirm that these are indeed METTL3 proteins, we repeated the western blot with a second anti-METTL3 antibody raised against amino acids surrounding Leu297 of METTL3, which correspond to amino acids encoded by exon 4. Again, we found the same bands in the exon2 *Mettl3* KO cell lines (S1A and S1C Fig). These proteins may have escaped notice in the original study as the study used a different antibody, which may have been unable to detect these isoforms [4]. Overall, the new METTL3-antibody-reactive proteins suggests that smaller METTL3 isoforms are produced in the exon2 *Mettl3* KO cells that may be the source of m⁶A in these cells. Although expression levels of these proteins appear low, previous studies have suggested that METTL3 is not rate limiting, and therefore, low METTL3 expression can still lead to high m⁶A levels [22].

We wanted to understand the mechanism of METTL3 expression in the exon2 *Mettl3* KO mESCs. To do this, we first determined the sequence of these isoforms. Since the exon2 *Mettl3* KO cells were produced using guide RNAs targeting exon 2 of *Mettl3* [4], any CRISPR/Cas9-induced mutations and potential alternative splicing events are likely to be in the 5' end

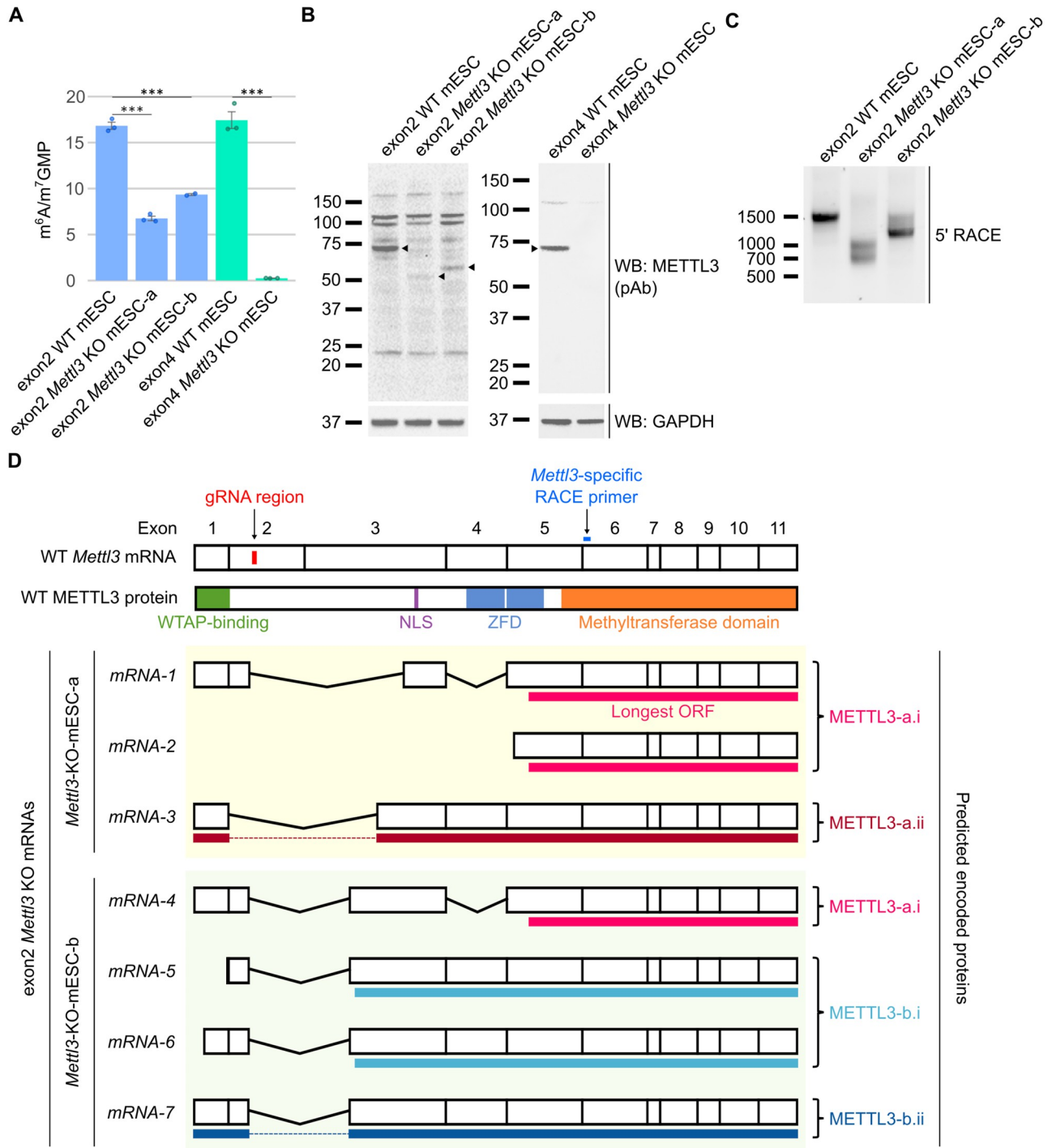


Fig 1. Previously described *Mettl3* KO mESC lines express shorter isoforms of *Mettl3*. (A) *Mettl3* KO mESCs from two groups have different m⁶A levels. To reconfirm the m⁶A levels using quantitative methods, we performed mass spectrometry to estimate the m⁶A in mRNA. Exon2 *Mettl3* KO mESCs show persistence of 40.2% (exon2 *Mettl3* KO mESC-a) and 55.6% (exon2 *Mettl3* KO mESC-b) m⁶A, respectively, while exon4 *Mettl3* KO mESCs show 1.45% m⁶A compared to WT. This confirms that exon4 *Mettl3* KO mESCs have near-complete loss of m⁶A, but not the exon2 *Mettl3* KO mESCs. Error bars indicate standard error ($n = 3$ for all, except $n = 2$ for exon2 *Mettl3* KO mESC-b). * = p -value < 0.5, ** = p -value < 0.01, *** = p -value < 0.005, n.s. = not significant. Underlying data can be found in S1 Data. (B) Exon2 *Mettl3* KO mESCs exhibit new anti-METTL3-immunoreactive bands. To investigate the effectiveness of the *Mettl3* knockout, we measured the loss of METTL3 via WB. Full-length METTL3 (75 kDa, arrowhead) was lost in both KO cell lines, but new bands, which were reactive to the anti-METTL3-antibody, appeared at approximately 50 kDa in exon2 *Mettl3* KO mESC-a and approximately 55 kDa in exon2 *Mettl3* KO mESC-b (arrowheads). This indicates the possibility that a novel smaller METTL3 protein was expressed in the exon2 *Mettl3* KO mESCs. In contrast, exon4 *Mettl3* KO mESCs have no proteins reactive to anti-METTL3-antibodies. 30 μ g per lane. (C) 5' RACE reveals the expression of shorter *Mettl3* mRNAs in the *Mettl3* KO mESCs. We used 5' RACE to

identify novel *Mettl3* mRNAs in the *Mettl3* KO mESCs. The full-length RACE product (approximately 1,500 bp) was lost in the *Mettl3* KO cells, but novel products at approximately 1,000 bp and approximately 700 bp were found in exon2 *Mettl3* KO mESC-a and at approximately 1,500 bp and approximately 1,300 bp in exon2 *Mettl3* KO mESC-b. These shorter mRNAs may encode the smaller METTL3 proteins seen in the KO cells. (D) Sequencing of 5' RACE products show *Mettl3* mRNAs with exon skipping or alternative transcription-start sites. We sequenced the 5' RACE products to characterize the *Mettl3* mRNA transcripts that are expressed by the exon2 *Mettl3* KO mESCs. All *Mettl3* mRNAs expressed in the KO cells skipped the guide RNA deletion region by exon skipping, or by using alternative transcription-start sites downstream of the deletion. The longest ORFs that are in-frame with the WT *Mettl3* mRNAs are shown as solid lines below each mRNA. The encoded protein is also represented, with the domains required for METTL3 activity shown. m⁶A, N⁶-methyladenosine; mESC, mouse embryonic stem cell; NLS, nuclear localization signal; ORF, open reading frame; pAb, polyclonal antibody; RACE, rapid amplification of cDNA ends; WB, western blot; WT, wild-type; ZFD, zinc finger domain.

<https://doi.org/10.1371/journal.pbio.3001683.g001>

of the transcript. We therefore used 5' RACE (rapid amplification of cDNA ends) [38] to identify new transcription-start sites or possible exon skipping events of the *Mettl3* transcripts expressed in these cells.

Using 5' RACE, a single major approximately 1,500 bp band was seen for *Mettl3* in WT mESCs (Fig 1C). In contrast, in the two exon2 *Mettl3* KO cell lines, we found shorter bands indicative of *Mettl3* mRNAs with a shorter 5' region (Fig 1C). We sequenced these 5' RACE products and found several *Mettl3* mRNAs from the exon2 *Mettl3* KO cells (Fig 1D and S1 Table). In all cases, the mRNAs show alternative splicing that bypasses the CRISPR deletion in exon 2 by exon skipping, or use of an alternative transcription-start site downstream of the deletion.

We next asked if these mRNAs could potentially encode the altered METTL3 proteins detected in the *Mettl3* KO mESCs. For each mRNA, we identified the longest possible open reading frame (ORF) that is in frame with the METTL3 catalytic domain (Fig 1D and S2 Table). In the case of *Mettl3* KO mESC-a, we found a transcript that is predicted to encode a METTL3 protein (designated "METTL3-a.ii") that matches the size of the altered METTL3 protein from this cell line (Fig 1B and 1D). Similarly, we identified a transcript that is predicted to encode a protein with a similar size to the altered METTL3 protein in *Mettl3* KO mESC-b (designated "METTL3-b.ii") (Fig 1B and 1D).

Together, these data identify potential transcripts that may encode the altered METTL3 proteins found in the exon2 *Mettl3* KO cells.

Altered METTL3 proteins expressed in incomplete *Mettl3* knockout mESCs can catalyze the formation of m⁶A in cells

We next asked if the novel *Mettl3* transcript isoforms encode functional m⁶A-forming methyltransferases. METTL3 contains several domains necessary for methyltransferase activity, including the WTAP-binding domain [39], the ZFD [19,36], and the methyltransferase domain [19,20]. Both METTL3-a.ii and METTL3-b.ii contain all 3 domains, and therefore may be functional. Other altered *Mettl3* transcripts in the *Mettl3* KO mESCs encode predicted proteins (designated "METTL3-a.i" and "METTL3-b.i") that lack one or more of these domains (Fig 2A). Notably, the methyltransferase domain is required for interaction with METTL14 [20,39], and METTL3 stabilizes METTL14 through this interaction [6,19]. The exon4 *Mettl3* KO mESCs were shown to have complete loss of METTL14 protein, supporting that METTL3 is required for METTL14 stability [5]. On the other hand, the exon2 *Mettl3* KO mESCs were shown to continue to express METTL14 [4], again suggesting that they express a METTL3 protein that was able to interact with and stabilize METTL14.

To test the activity of these METTL3 isoforms, we expressed FLAG-tagged METTL3 isoform constructs in the exon4 *Mettl3* KO mESCs, which lack METTL3-immunoreactive bands (Figs 1B, S1B and S1C) and lack m⁶A in mRNA (Fig 1A). First, we noted that the size of

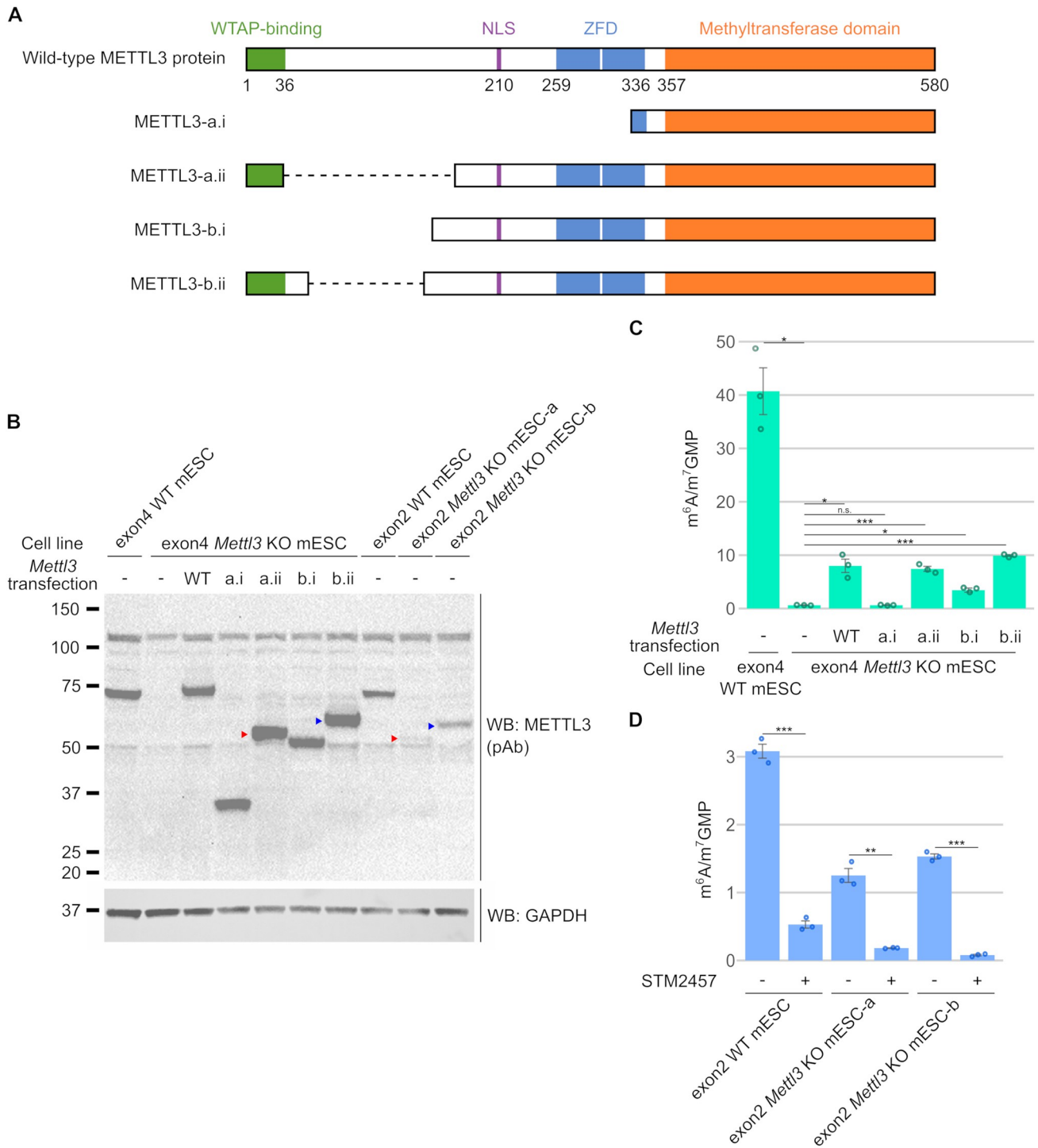


Fig 2. Shortened isoforms of METTL3 catalyze m⁶A formation in *Mettl3* KO mESCs. (A) The predicted domain structure of proteins encoded by the altered METTL3 ORFs expressed in exon2 *Mettl3* KO mESCs suggests they may be functional. The domains that are known to be necessary for m⁶A formation by METTL3 include the WTAP-binding domain [39], ZFD [19,36], and methyltransferase domain [19,20]. To determine if the METTL3 ORFs from exon2 *Mettl3* KO mESCs encode functional METTL3 proteins, we predicted the domain structure of the METTL3 protein isoforms from their ORFs. While all the predicted proteins have the methyltransferase domain, only METTL3-a.ii and METTL3-b.ii have all the known critical domains for m⁶A-writing. (B) WB of transfected FLAG-tagged METTL3 isoform ORFs. To determine if the METTL3 ORFs we found in the knockout cells can synthesize m⁶A, we expressed the METTL3 ORFs in exon4 *Mettl3* KO mESCs that exhibit no METTL3 protein and essentially no baseline m⁶A signal. After 48 h, the alternatively spliced METTL3 proteins can be detected by immunoblotting with an anti-METTL3 antibody. FLAG-METTL3-a.ii (50 kDa, red arrowhead) and FLAG-METTL3-b.ii (55 kDa, blue arrowhead) have similar sizes to the anti-METTL3-antibody-reactive protein seen in exon2 *Mettl3* KO mESC-a (red arrowhead) and exon2 *Mettl3* KO mESC-b (blue arrowhead), respectively. 30 μg per lane. (C) Isoforms of METTL3 proteins can write

m⁶A. After 48 h of transfection, RNA from each sample was processed, and m⁶A was measured using mass spectrometry. Expression of full-length WT METTL3 was able to rescue 19.7% of the m⁶A. METTL3-a.i was unable to rescue m⁶A, but METTL3-a.ii was able to rescue 18.3% of m⁶A. METTL3-b.i could only rescue 8.5% of m⁶A, whereas METTL3-b.ii rescued 24.4% of m⁶A, respectively. Thus, METTL3-a.ii and METTL3-b.ii proteins that are expressed in the exon2 *Mettl3* KO mESCs are able to catalyze the formation of m⁶A. Error bars indicate standard error ($n = 3$). * = p -value < 0.05, ** = p -value < 0.01, *** = p -value < 0.005, n.s. = not significant. Underlying data can be found in [S1 Data](#). (D) A METTL3-specific inhibitor leads to loss of m⁶A even in exon2 *Mettl3* KO mESCs. Exon2 WT and *Mettl3* KO mESCs were treated with 30 μ M STM2457, a METTL3-specific inhibitor, and m⁶A levels were measured by mass spectrometry after 48 h. STM2457 treatment reduced m⁶A by 82.8% in the WT mESCs. In exon2 *Mettl3* KO mESC, m⁶A was reduced by 85.4% in *Mettl3* KO mESC-a after STM2457 treatment and by 94.8% in *Mettl3* KO mESC-b. Thus, METTL3 is responsible for the remaining m⁶A in the exon2 *Mettl3* KO mESCs. Residual m⁶A after STM2457 treatment may reflect incomplete inhibition of METTL3 at 30 μ M. Error bars indicate standard error ($n = 3$). * = p -value < 0.05, ** = p -value < 0.01, *** = p -value < 0.005, n.s. = not significant. Underlying data can be found in [S1 Data](#). m⁶A, N⁶-methyladenosine; mESC, mouse embryonic stem cell; NLS, nuclear localization signal; ORF, open reading frame; pAb, polyclonal antibody; WB, western blot; WT, wild-type; ZFD, zinc finger domain.

<https://doi.org/10.1371/journal.pbio.3001683.g002>

METTL3-a.ii and METTL3-b.ii were indeed similar to the sizes of the smaller METTL3 proteins in *Mettl3* KO mESC-a and *Mettl3* KO mESC-b, respectively ([Fig 2B](#)). Thus, METTL3-a.ii and METTL3-b.ii may be the novel METTL3 isoforms we detected in the exon2 *Mettl3* KO mESCs. In contrast, bands corresponding to METTL3-a.i (approximately 30.4 kDa) and METTL3-b.i (approximately 49 kDa) were not seen in *Mettl3* KO mESC-a or *Mettl3* KO mESC-b, respectively ([Figs 1B](#) and [2B](#)). These METTL3 isoforms may have been less efficiently transcribed or translated, or may be less stable, leading to the lack of an immunoreactive band for these proteins.

We first tested expression of full-length METTL3 in the exon4 *Mettl3* KO mESCs and found that they rescued m⁶A levels to 19.7% of WT ([Fig 2C](#)). The lack of complete rescue by the WT *Mettl3* transcript may be due to inefficient or uneven transfection of the cell population ([S2 Fig](#)). METTL3-a.ii and METTL3-b.ii were able to rescue 18.3% and 24.4% of the m⁶A, respectively ([Fig 2C](#)), suggesting that they are functional m⁶A methyltransferases. As predicted, METTL3-a.i failed to rescue m⁶A and METTL3-b.i could only rescue a small portion of m⁶A (8.5%) ([Fig 2C](#)). Overall, these data indicate that the exon2 *Mettl3* KO mESCs express hypomorphic *Mettl3* alleles that encode catalytically active METTL3 isoforms, METTL3-a.ii and METTL3-b.ii. Thus, the exon2 *Mettl3* KO mESCs should be viewed as incomplete knock-outs with hypomorphic *Mettl3* alleles.

We wanted to find out if the mRNAs encoding METTL3-a.ii and METTL3-b.ii were translated in the cells to produce their respective proteins. To test this, we performed polysome profiling on the exon2 *Mettl3* KO mESCs. We collected fractions corresponding to submonosomal, light polysome, medium polysome, and heavy polysome fractions ([S3 Fig](#)). Using PCR primers, we amplified *Mettl3* transcript isoforms in each fraction. We found *Mettl3* PCR amplification products in the heavy polysome fraction ([S3 Fig](#)). Sequencing confirmed that these PCR products are *mRNA-3* that encodes METTL3-a.ii in *Mettl3* KO-mESC-a and *mRNA-7* that encodes METTL3-b.ii in *Mettl3* KO mESC-b ([S3 Fig](#) and [S3 Table](#)). Thus, these transcripts are indeed translated.

We also used an orthogonal pharmacological approach to determine if a METTL3 isoform could be responsible for the m⁶A produced in the exon2 *Mettl3* KO mESCs. STM2457 is a METTL3 inhibitor that was developed by a structure-based approach to be highly specific to METTL3 [[40](#)]. Screens with other methyltransferases showed that STM2457 does not affect the activity of other known RNA methyltransferases [[40](#)]. Thus, we treated the exon2 *Mettl3* KO cells with STM2457 to investigate if the remaining m⁶A in these cells was produced by METTL3. STM2457 treatment reduced m⁶A levels in the WT mESCs by 82.8% after 48 h ([Fig 2D](#)). Similarly, we saw that STM2457 treatment reduced m⁶A by 85.4% in exon2 *Mettl3* KO mESC-a and 94.8% in exon2 *Mettl3* KO mESC-b ([Fig 2D](#)), indicating that this m⁶A was produced by METTL3. The small amount of remaining m⁶A could be either due to incomplete

inhibition by STM2457, or a small amount of m⁶A catalyzed by a different methyltransferase. On the other hand, STM2457 treatment had no effect on m⁶A levels in the exon4 *Mettl3* KO mESCs (S4 Fig). This suggests that METTL3 is indeed responsible for the remaining m⁶A in the exon2 *Mettl3* KO mESCs.

***METTL3* knockout U2OS cells express an altered METTL3 protein**

The idea that METTL3 is not responsible for all m⁶A in mRNA was further supported by *METTL3* knockout in several cell lines, each of which show high residual levels of m⁶A [23–29]. For example, a *METTL3* KO U2OS cell line was reported to have approximately 60% of the m⁶A remaining compared to WT [23,24]. Similarly, we found that a previously reported *METTL3* KO A549 cell line [41] has approximately 90% of m⁶A remaining compared to the WT (S5 Fig). The persistence of m⁶A in these *METTL3* knockout cell lines has led to the idea that other enzymes mediate a substantial fraction of m⁶A in mRNA. However, in light of our finding that alternatively spliced *Mettl3* isoforms were induced in the *Mettl3* knockout mESCs, another possibility is that *METTL3* isoforms were induced in these *METTL3* knockout cell lines as well, which led to the high m⁶A levels in these *METTL3* knockout cell lines.

We examined one of these cell lines—the *METTL3* knockout U2OS cell line that was generated using CRISPR/Cas9-directed mutagenesis with a guide RNA targeting exon 1 [23]. We first reconfirmed the m⁶A levels in these *METTL3* knockout cells and found that the *METTL3* knockout U2OS cells retained 75.2% m⁶A compared to the WT (Fig 3A), comparable to the 60% originally reported [24]. Hence, *METTL3* knockout U2OS cells continue to have high levels of m⁶A in mRNA.

We next asked if the *METTL3* KO U2OS cells express a METTL3 protein using a western blot. We observed full-length METTL3 in the WT U2OS cells, but not in the knockout cells (Fig 3B). However, a slightly larger anti-METTL3 immunoreactive band was detected exclusively in the knockout cells (Fig 3B). To confirm that this is indeed a METTL3 isoform, we validated the western blot with a second anti-METTL3 monoclonal antibody and found that the protein in the knockout cells was also reactive to the second anti-METTL3 antibody (Fig 3C). We note that we could observe a similar protein band in the authors' original western blot that used a different METTL3 antibody [23]; however, it was much fainter and could easily be mistaken for nonspecific background. Thus, this suggests that the *METTL3* KO U2OS cells continued to express a METTL3 protein.

We wanted to find out if METTL3 could be responsible for the m⁶A produced in the *METTL3* KO U2OS cells using the METTL3-specific inhibitor, STM2457 [40]. STM2457 treatment reduced m⁶A levels in the WT U2OS cells by 89.8% after 48 h (Fig 3D). Similarly, STM2457 treatment reduced m⁶A levels by 92.1% in the *METTL3* KO U2OS cells (Fig 3D). These data suggest that a METTL3 isoform is responsible for most of the remaining m⁶A in the *METTL3* KO U2OS cells. Furthermore, the depletion of approximately 90% m⁶A by STM2457 further suggests that METTL3 is responsible for the majority of m⁶A in U2OS cells. Overall, this data again suggests that CRISPR/Cas9 mutagenesis results in the appearance of a novel METTL3 isoform in a *METTL3* knockout cell line, which could explain m⁶A persistence in these cells.

***METTL3* knockout cell lines are generally not viable**

Several *METTL3* knockout cell lines have been reported despite the fact that *METTL3* is thought to be an essential gene. *Mettl3* knockout is embryonic lethal in mice at E5.5 before cell specification occurs [5], and CRISPR screens have indicated that *METTL3* is an essential gene in specific cell lines that were tested [7,42]. On the other hand, the exon4 *Mettl3* knockout

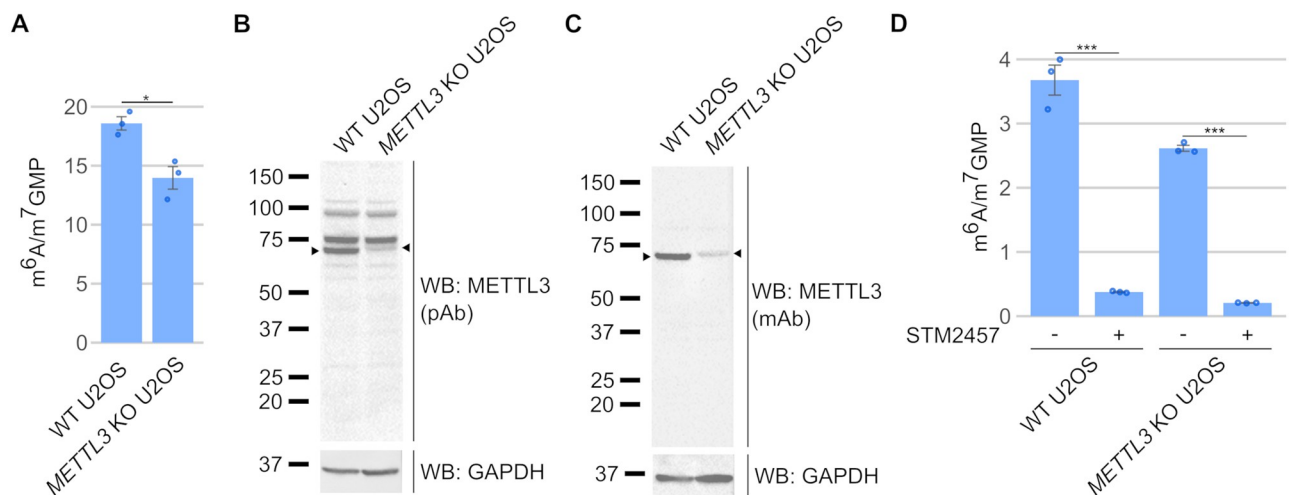


Fig 3. *METTL3* knockout in U2OS cells also appears to be incomplete. (A) *METTL3* KO U2OS cells have persistent m⁶A. *METTL3* KO U2OS cells have been reported to have 60% the levels of m⁶A found in control U2OS cells [24]. We reconfirmed this with mass spectrometry measurements of m⁶A, which showed that *METTL3* KO U2OS cells have 75.2% remaining m⁶A compared to WT. Thus, m⁶A levels remain high in *METTL3* KO U2OS cells. Error bars indicate standard error ($n = 3$). * = p -value < 0.5, ** = p -value < 0.01, *** = p -value < 0.005, n.s. = not significant. Underlying data can be found in [S1 Data](#). (B) *METTL3* KO U2OS cells express a novel anti-*METTL3*-antibody-reactive protein. As m⁶A levels were not completely ablated in the *METTL3* KO U2OS cells, we assessed *METTL3* protein expression in these cells to confirm if the knockout was effective. We found that WT *METTL3* protein was lost in the *METTL3* KO U2OS cells, but a larger protein that was reactive to the anti-*METTL3* antibody was found in the *METTL3* KO U2OS cells. This suggests the *METTL3* KO U2OS cells express a novel *METTL3* protein that is slightly larger than the WT *METTL3*. (C) Confirmation of a novel *METTL3*-like protein in *METTL3* KO U2OS using a second *METTL3* antibody. To confirm that the *METTL3*-immunoreactive band we saw in *METTL3* KO U2OS cells in [Fig 3B](#) was *METTL3*, we used a second anti-*METTL3* mAb to confirm the result. The same protein band is immunoreactive to the second anti-*METTL3* antibody, thus suggesting that the *METTL3* KO U2OS cells express a novel, larger *METTL3* protein. (D) A *METTL3*-specific inhibitor leads to loss of m⁶A even in *METTL3* KO U2OS cells. WT and *METTL3* KO U2OS cells were treated with 30 μ M STM2457, and m⁶A levels were measured by mass spectrometry after 48 h. m⁶A was reduced by 89.8% in the WT U2OS cells and 92.1% in the *METTL3* KO U2OS cells after STM2457 treatment. It should be noted that 30 μ M may not fully inhibit *METTL3*, so some of the residual m⁶A after STM2457 treatment may still derive from *METTL3* isoforms. Thus, a *METTL3* isoform is responsible for most of the remaining m⁶A in the *METTL3* KO U2OS cells. Error bars indicate standard error ($n = 3$). * = p -value < 0.5, ** = p -value < 0.01, *** = p -value < 0.005, n.s. = not significant. Underlying data can be found in [S1 Data](#). mAb, monoclonal antibody; m⁶A, N⁶-methyladenosine; pAb, polyclonal antibody; WB, western blot; WT, wild-type.

<https://doi.org/10.1371/journal.pbio.3001683.g003>

mESCs are able to survive, demonstrating that some cell lines can survive without *METTL3* or m⁶A. Therefore, it is not clear which cell lines require *METTL3* for survival. If *METTL3* is required for survival of most cell lines, it would cast doubt on the stable *METTL3* knockout cell lines that have been reported in the literature.

To understand which cell lines require *METTL3* for survival, we screened the Cancer Dependency Map Project (DepMap) 21Q4 dataset [43–47]. This dataset measures cell proliferation in 1,054 cell lines following a CRISPR loss-of-function screen. Failure of a cell line to grow after expression of the guide RNA that inactivates a gene indicates that the gene is essential in the cell line. The probability that a cell line is dependent on each gene is calculated as a gene dependency probability score, which accounts for guide efficacy as well as copy number of each gene. The 21Q4 DepMap dataset [47] showed that *METTL3* is necessary for cell proliferation in 801 of 1,054 tested cell lines ([Fig 4A](#)). To account for the possibility of off-target effects in the DepMap CRISPR screen, we further looked for *METTL3*-dependent cell lines that were also dependent on other members of the writer complex, *METTL14* and *WTAP* [6,21,22,48]. We found that of the 801 cell lines dependent on *METTL3*, 683 were also dependent on *METTL14* and *WTAP* ([S6 Fig](#)), suggesting that these cell lines indeed require the m⁶A methyltransferase complex for proliferation. The *METTL3*-dependent cell lines include the U2OS and A549 cell lines that other groups have used to make *METTL3* knockout cell lines

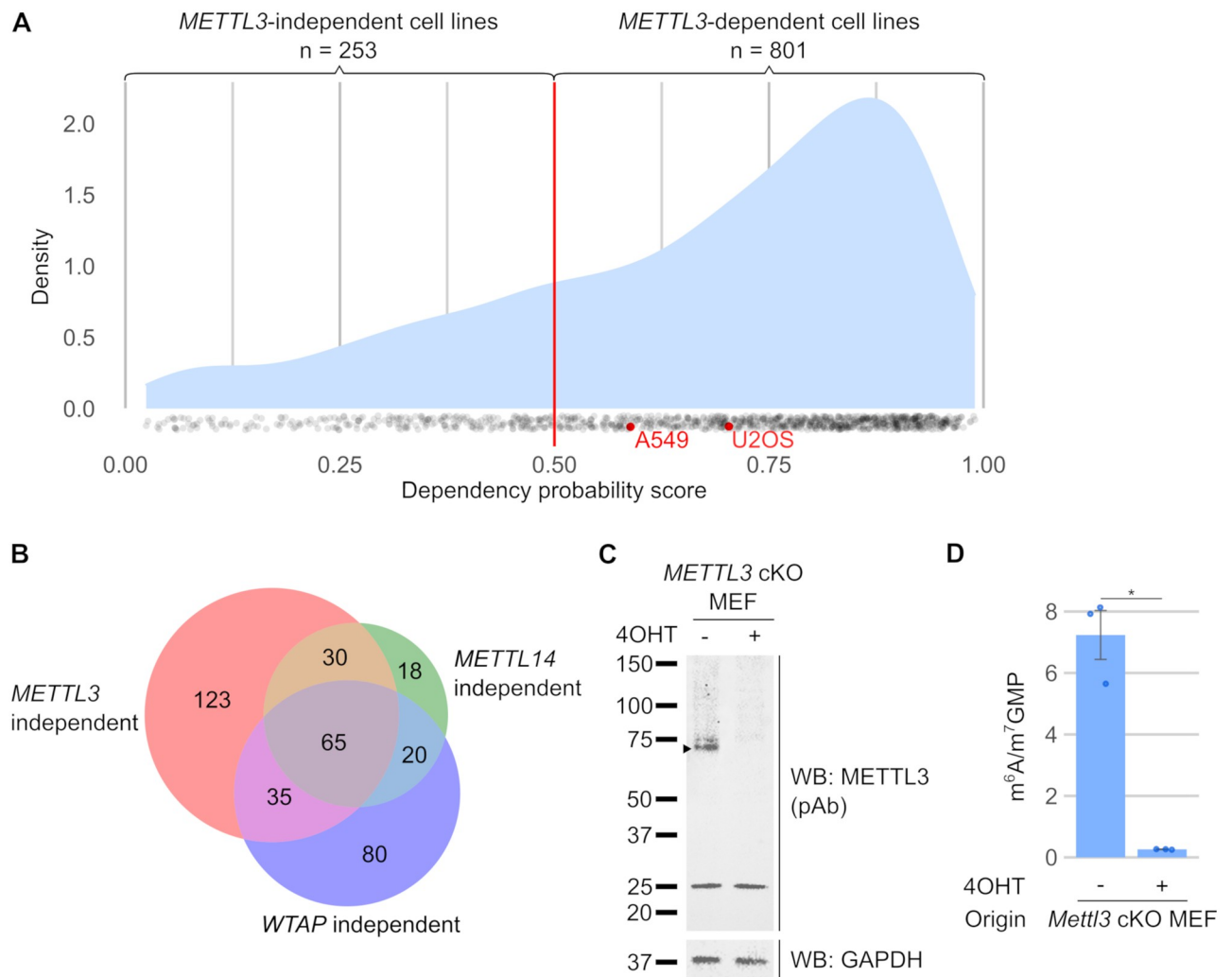


Fig 4. Conditional *METTL3* knockouts can be used to study m⁶A when stable *METTL3* knockouts are not viable. (A) Most cell lines are dependent on *METTL3* for growth. Mouse studies previously indicated that *Mettl3* is an essential gene for early embryonic survival [5], so we wanted to know which cell lines are dependent on *METTL3*. Using the CRISPR gene dependency probability score from the DepMap 21Q4 dataset [43–47], we found that 801 of 1,054 cell lines are dependent on *METTL3* (dependency probability score >0.5). Therefore, most cell lines will not survive after *METTL3* knockout. The density plot shows the overall distribution of dependency probability scores, while each individual cell line is represented as a dot. U2OS and A549 cell lines (red), where *METTL3* has been previously knocked out, are shown here to be dependent on *METTL3* and thus should not be viable after *METTL3* knockout. Underlying data for this figure was extracted from the DepMap 21Q4 dataset [47]. (B) A small subset of cell lines may be m⁶A independent. Although most cell lines are dependent on *METTL3*, a small subset of cell lines can survive despite *METTL3* knockout. To identify cell lines that we can confidently consider m⁶A-independent, we obtained a list of cell lines whose survival is also independent of other members of the m⁶A writer complex, *METTL3*, *METTL14*, and *WTAP*. This approach suggests that 65 cell lines may be able to proliferate in an m⁶A-independent manner (S4 Table). Underlying data for this figure was extracted from the DepMap 21Q4 dataset [47]. (C) *Mettl3* conditional knockout MEFs do not express *METTL3* protein. To determine the amount of m⁶A in mRNA that can be attributed to *Mettl3*, we generated a tamoxifen-inducible *Mettl3* conditional knockout MEF cell line. We used WB to validate the loss of *METTL3*. After 5 days of 4-hydroxytamoxifen treatment (500 nM), we observed loss of the WT *METTL3* protein. 30 µg per lane. (D) *Mettl3* conditional knockout MEFs show near-complete loss of m⁶A. We measured m⁶A levels in mRNA derived from tamoxifen-inducible *Mettl3* conditional knockout MEFs. Eight days after 4OHT treatment (500 nM), the *Mettl3* KO MEFs showed 3.6% remaining m⁶A. Hence, m⁶A is almost completely lost after *Mettl3* knockout in MEFs. Error bars indicate standard error (n = 3). * = p-value < 0.5, ** = p-value < 0.01, *** = p-value < 0.005, n.s. = not significant. Underlying data can be found in S1 Data. m⁶A, N⁶-methyladenosine; MEF, mouse embryonic fibroblast; pAb, polyclonal antibody; WB, western blot; 4OHT, 4-hydroxytamoxifen.

<https://doi.org/10.1371/journal.pbio.3001683.g004>

[23,41] (Fig 4A). The DepMap data suggests that these reported *METTL3* cell lines should not have been viable.

It is important to note that the DepMap dataset measures proliferation after a CRISPR loss-of-function screen. Even if a small number of cells manage to escape the CRISPR inactivation of *METTL3* and continue to proliferate, the overall reduction in proliferation will still be reflected in the DepMap gene dependency score. On the other hand, during generation of *METTL3* knockout cell lines, researchers are actively selecting for cells that continue to proliferate, therefore potentially selecting for cells that have escaped the knockout.

Thus, this leads us to believe that reported stable *METTL3* knockout cell lines were able to survive because they were selected for their ability to produce a functional alternatively spliced *METTL3* isoform that bypasses the CRISPR mutation, similar to the exon2 *Mettl3* KO mESCs. This alternative *METTL3* isoform also explains why these cells retain high levels of m⁶A. Thus, the reported *METTL3* knockout cell lines are likely not true *METTL3* knockouts.

However, a few cell lines are able to survive after *METTL3* knockout. The exon4 *Mettl3* KO mESCs are one such example of a cell that can survive without *METTL3* [5]. A group has also reported that mouse CD4+ T cells can survive after *Mettl3* deletion [30]. The 21Q4 DepMap dataset shows that only 253 cell lines are not dependent on *METTL3*. Furthermore, only 65 cell lines were not dependent on any of the members of the m⁶A writer complex, which includes *METTL3*, *METTL14*, and *WTAP* [6,21,22,48] (Fig 4B and S4 Table). This small subset of cell lines may be the best cell lines for creating *METTL3* knockout cells, since loss of m⁶A in the other cell lines will most likely lead to cell death unless an alternatively spliced *METTL3* isoform is selected for. Thus, any reported stable *METTL3* knockout in cell lines other than this small subset of m⁶A-independent cell lines should be more carefully evaluated.

METTL3 is responsible for all m⁶A in mRNA in mouse embryonic fibroblasts

Although the full *Mettl3* knockout in mESCs led to near complete loss of m⁶A [5], this may be a unique feature of embryonic stem cells. It is possible that other cell types can compensate for *METTL3* depletion using other methyltransferases that can synthesize m⁶A. To find out if *METTL3* is the major writer of m⁶A in mRNA in cell lines other than mESCs, we needed to deplete *METTL3* in a different cell line, and measure the remaining amount of m⁶A. Because stable *METTL3* knockout cells are generally not viable, we produced *Mettl3* conditional knockout mouse embryonic fibroblast (MEF) cell lines derived from *Mettl3*^{lox/lox} mice. *loxP* sites flanking exon 4 of *METTL3* were inserted in the mouse genome [32]. Upon tamoxifen-induced expression of Cre, recombination of the *loxP* sites leads to deletion of exon 4 that encodes the ZFD, similar to how *Mettl3* is deleted in the exon4 *Mettl3* KO mESCs [5].

Using the tamoxifen-inducible *Mettl3* knockout MEFs, we found that *METTL3* protein expression was completely lost 5 days after tamoxifen treatment (Figs 4C and S7A). By day 6, we observed that MEF proliferation was markedly reduced (S7B Fig), corroborating that *METTL3* is essential for proliferation, and therefore stable *METTL3* knockout cell lines are unlikely to survive.

We next determined the fraction of m⁶A in mRNA that is catalyzed by *METTL3* in MEFs. We found that 8 days after tamoxifen treatment, most of the m⁶A was lost, with only 3.6% of m⁶A remaining (Fig 4D). Thus, this demonstrates that aside from mESCs, *METTL3* is also the predominant m⁶A methyltransferase in MEFs.

Discussion

Here, we address the source of METTL3-independent m⁶A, which is widely discussed in the literature and have been described based on high levels of residual m⁶A after knockdown or knockout of *METTL3* [4,6–8,21–32,41,42,48–52]. This has led to the idea that some m⁶A is catalyzed by METTL3, while another substantial fraction of m⁶A is catalyzed by other enzymes. Our results show that the residual m⁶A seen after *METTL3* knockout can be readily explained by the induction of alternatively spliced hypomorphic *METTL3* alleles and the subsequent expression of altered METTL3 proteins. We show that a widely used “*Mettl3* knockout” mESC line [4] undergoes alternative splicing to bypass the CRISPR/Cas9-induced mutations, creating a smaller but catalytically active METTL3 protein. We further show that another published *METTL3* knockout U2OS cell line that also has been shown to contain high levels of residual m⁶A [23,24] also exhibits an altered METTL3 protein. These studies show that altered METTL3 proteins likely account for the residual m⁶A in the cells, rather than an alternative methyltransferase. The evidence for the importance of METTL3 alone as the major m⁶A-forming enzyme is supported by our data in which deleting *METTL3* in MEFs using a large exon 4 deletion leads to a loss of >95% of m⁶A, and by our data where METTL3 inhibition by STM2457 lead to 90% loss of m⁶A in U2OS cells. Lastly, we demonstrate that METTL3 is essential for the proliferation and growth of the vast majority of cell lines and therefore, many reported stable *METTL3* knockout cell lines are unlikely to be true knockout cells since they would not be able to proliferate, with a few exceptions. Overall, our studies resolve an important long-standing inconsistency in the literature and argue that (1) METTL3 is the major source of m⁶A in mRNA; and (2) m⁶A that remains after *METTL3* knockout is likely due to cells escaping *METTL3* deletion by creation of new *METTL3* isoforms.

Our data suggests that *METTL3* knockout can be validated by measuring residual m⁶A levels in mRNA. We have shown here that several cell lines described to be *METTL3* knockouts still express METTL3 isoforms and have high levels of m⁶A [23–29]. *METTL3* knockout cells that continue to have m⁶A should not be used to determine the function of m⁶A in any biological process. Because these cells retain considerable amounts of m⁶A, they cannot be used to identify pathways and processes that require m⁶A. Furthermore, these cells may express isoforms of METTL3 with unknown functions and properties. These nonphysiological METTL3 isoforms may lead to unexpected results, which may be conflated with findings that arise from loss of m⁶A. We note that we observed multiple unique METTL3 isoforms in the different cell lines we characterized, all of which are not visible in the WT cells. These METTL3 isoforms are likely to have been generated by stochastic alternative splicing events, which were eventually selected for as the production of a functional METTL3 gave the cell a proliferative advantage. Thus, each CRISPR knockout cell line may produce different METTL3 isoforms, each with unique unpredictable properties.

To more reliably inactivate *METTL3*, genomic regions encoding critical enzymatic domains should be deleted, rather than simply mutated, since small mutations may be more readily bypassed through alternative splicing events. Furthermore, as *METTL3* knockout is not viable in most cell lines, conditional *METTL3* knockouts provide a useful model for studying m⁶A. *METTL3* deletion and m⁶A levels must be carefully documented before reporting these cell lines as *METTL3* knockouts. m⁶A quantification will also allow a better understanding if partial or complete losses of m⁶A are able to mediate the studied outcomes.

Although our results indicate that METTL3 accounts for the vast majority (>95%) of m⁶A in mRNA in MEFs and mESCs, numerous studies have shown that *METTL3* knockout results in a large amount of residual m⁶A in mRNA. Three major technical problems likely account for this “METTL3-independent” m⁶A:

1. Hypomorphic *METTL3* alleles. In this study, we characterized a variety of diverse alternative splicing events that occur in “*Mettl3* knockout” mESCs. In these cells, *Mettl3* was targeted using CRISPR/Cas9 systems to create indels and frameshifts. Although this is a reasonable method for gene inactivation [53,54] and may have initially inactivated *Mettl3*, cells which develop alternative splicing patterns that enable formation of an active METTL3 enzyme will gain a proliferative advantage. It is likely that after *METTL3* knockout, cells in which *METTL3* was truly inactivated will stop proliferating. At the same time, any cells that can express a *METTL3* isoform that skips the mutation will gain a proliferative advantage, and will be further selected for their ability to up-regulate this isoform. These escaped cells will then be expanded and incorrectly reported as a “*METTL3* knockout” cell line. Similar alternative splicing events that bypass CRISPR/Cas9-induced mutations have been reported in studies of inactivation of other genes [55–57]. Alternative splicing may allow bypass of CRISPR/Cas9-mediated *METTL3* knockout in other cell lines.
2. Heterogeneity of cell population. In a population of *METTL3* knockout cells, any contaminating cells that express functional METTL3 will lead to some level of m⁶A being produced and detected. For example, mouse studies frequently use tissue-specific knockout systems to deplete *Mettl3* in a specific tissue as *Mettl3* knockout is embryonic lethal [5,30–32]. When isolating these tissues, contamination from other cells in the tissue, such as endothelial or immune cells, could lead to detectable m⁶A levels in the samples. Additionally, Cre expression is variable, and can lead to a lack of knockout in some cells [58]. Thus, residual m⁶A in these experiments may simply reflect a mixed population of knockout and non-knockout cells. METTL3 levels can be measured by immunofluorescence to determine if knockout is heterogeneous in these populations.
3. Misattribution of background noise in m⁶A mapping studies as m⁶A sites. A common approach for studying m⁶A sites is MeRIP-seq [3,59], and other antibody-based sequencing methods to detect m⁶A across the transcriptome [60]. In numerous studies, researchers knocked down or deleted *METTL3* and regarded the remaining m⁶A “peaks” as “METTL3-independent m⁶A peaks” [35,52,61]. However, several studies have shown that even in *METTL3* knockout cells where m⁶A cannot be detected, m⁶A peaks can still be observed [62–64]. Thus, these m⁶A peaks should be regarded as background noise, rather than “METTL3-independent m⁶A peaks.” This noise can be due to m⁶A antibodies binding to non-m⁶A sites [60,61,63] or due to nonspecific binding during immunoprecipitation [65]. Thus, peaks that remain after *METTL3* knockout likely do not reflect real m⁶A sites. To identify true METTL3-independent m⁶A, methods such as SCARLET [66] can be used to validate that an m⁶A site in *METTL3* knockout actually reflects m⁶A.

A very small amount of m⁶A clearly remains after *Mettl3* knockout in both the exon4 *Mettl3* KO mESCs and in our conditional *Mettl3* KO MEFs. This m⁶A appears to be resistant to the METTL3 inhibitor STM2457. An alternative methyltransferase may be able to produce m⁶A on a small number of mRNA transcripts. For example, METTL16, which catalyzes the formation of m⁶A in U6 snRNA, also methylates *MAT2A* mRNA [67,68]. However, the sequence context of METTL16 is CAG [69–71], which differs from the predominant DRACH (D = A/G/U, R = A/G, H = A/C/U) sequence context for METTL3 [60,72,73]. Furthermore, METTL16 methylation is dependent on a hairpin structure found in U6 snRNA and *MAT2A*. Although current attempts to find other METTL16-dependent m⁶A in mRNA have been unsuccessful [61,68], METTL16-dependent m⁶A can likely be recognized based on the CAG sequence context and the U6-like hairpin structural context. m⁶A can also be formed by METTL5-TRMT112 and ZCCHC4 in the 18S and 28S rRNA, respectively [74,75]. Although

current attempts have failed to identify m⁶A in mRNA catalyzed by these enzymes [74], a candidate m⁶A mediated by either of these enzymes will likely be in an AAC sequence context as well as the unique structural context utilized by these enzymes [74,76]. Any m⁶A predicted to be “METTL3-independent” is likely to exist within these unique structural contexts and would be lost upon depletion of one of these enzymes.

Importantly, our data does not negate the conclusions of the original studies by Batista and colleagues on the role of METTL3 in embryonic stem cell differentiation. Batista and colleagues used their *Mettl3* hypomorphic mESCs to show that m⁶A is required for differentiation from the naïve pluripotent stem cell state [4]. This result was later corroborated by Geula and colleagues using complete *Mettl3* knockout mESCs [5]. Although one should approach the initial study with caution due to the unknown effects of the hypomorphs, the study supports the idea that a partial depletion of m⁶A is sufficient to block differentiation of primed mESCs [5]. Thus, mESCs are highly sensitive to m⁶A levels and fail to differentiate even with partial loss of m⁶A. This has important implications for researchers attempting to inhibit METTL3 to influence cellular differentiation states, for example, in cancer [7,40].

Materials and methods

Cell culture

Exon2 *Mettl3* KO and WT mESCs were previously described by Batista and colleagues [4], and were a gift from P.J. Batista and H. Chang (Stanford University). Exon4 *Mettl3* KO and WT mESCs were previously described by Geula and colleagues [5], and were a gift from S. Geula and J.H. Hanna (Weizmann Institute of Science). All mESCs were grown in gelatinized (0.1% gelatin in water, EmbryoMax ES-006-B) tissue culture plates in mESC media (KnockOut DMEM (Gibco #10829018), 15% heat-inactivated fetal bovine serum (FBS) (Gibco #26140079), 100 U/ml penicillin, 100 µg/ml streptomycin (Gibco #15140122), 1× GlutaMax (Gibco #35050061), 55 µM β-mercaptoethanol (Gibco #21985023), 1× MEM non-essential amino acids (Gibco #11140076), 1,000 U/ml LIF (Millipore ESG1107), 3 µM CHIR99201 (Sigma Aldrich SML1046), 1 µM PD0325901 (APEX BIO A3013)).

METTL3 KO U2OS cells were previously described by Xiang and colleagues [23], and were a gift from Y. Xiang and Y. Shi (University of Oxford). *METTL3* KO A549 cells were previously described by Courtney and colleagues [41], and were a gift from D.G. Courtney and B.R. Cullen (Duke University Medical Center). U2OS cells and A549 cells were grown in high glucose DMEM (Gibco #11995073) with 10% FBS (Gibco #26140079) and 1% penicillin-streptomycin (Gibco #15140122).

All cells were grown at 37°C, 5.0% CO₂. All cells were passaged as needed using TrypLE Express (Gibco #12604013).

Mass spectrometry measurements of m⁶A

m⁶A measurements were performed using mass spectrometry as previously described [37]. Total RNA was extracted from cells using TRIzol Reagent (Invitrogen #15596026) and treated with 2 U RNase-free DNase I (New England Biolabs M0303) for 1 h. RNA was cleaned up using RNA Clean & Concentrator (Zymo R1017). RNA was decapped using yDcpS enzyme (New England Biolabs M0463) to release m⁷G caps as 7-methylguanosine-monophosphate (m⁷GMP), then digested using RNase T1 (Invitrogen AM2283) and S1 nuclease (Invitrogen #18001-016) in 1× mung bean nuclease buffer (New England Biolabs B0250) to release single nucleotides. Enzymes were precipitated out of solution using 4× volume of 100% methanol. No-RNase T1 samples were also prepared and measured as background controls for m⁶A.

Nucleic acids were quantified by liquid chromatography with tandem mass spectrometry (LC–MS/MS) using a platform comprised of an Agilent Model 1290 Infinity II liquid chromatography system coupled to an Agilent 6460 Triple Quadrupole mass spectrometer equipped with Agilent Jet Stream Technology. Two injections of 2 μ l each were performed for each sample, and the mean peak area was calculated from the 2 injections. m^6A and m^7GMP readings were taken from each injection. The m^6A reading represents the amount of m^6A in mRNA, while m^7GMP readings represent the number of mRNAs in each sample. Mean m^6A/m^7GMP data of 2 or 3 biological replicates is reported with standard error. We thank N. Attarwala, Q.Y. Chen, and S.S. Gross (Weill Cornell Medicine) for conducting all LC–MS/MS experiments.

Western blot

Cells were lysed in RIPA buffer (50 mM Tris-HCl (pH 7.5), 200 mM NaCl, 1% NP-40, 0.5% sodium deoxycholate, 0.1% SDS) with 1 \times Halt protease and phosphatase inhibitor cocktail (Thermo Scientific #78440). Cell debris was cleared by centrifuging at 14,000 G for 10 min. Protein quantification was done by Quick Start Bradford Protein assay (BioRad #5000201) or Pierce BCA protein assay kit (Thermo Scientific #23225) according to manufacturer's instructions. Protein samples were resuspended in 1 \times NuPAGE LDS Sample Buffer (Invitrogen NP0007) + 50 mM dithiothreitol. Protein samples were separated by electrophoresis using NuPage 4% to 12% Bis-Tris gels (Invitrogen NP0322, NP0335) alongside Precision Plus Protein All Blue Prestained Protein Standards (Bio-Rad #1610373). Proteins were then transferred to nitrocellulose membranes in 1 \times Tris-glycine transfer buffer (25 mM Tris base, 200 mM glycine) + 20% methanol. Membranes were blocked using 5% BSA in phosphate buffered saline (PBS) + 0.1% (v/v) Tween-20 for 1 h at room temperature, then stained with primary antibodies overnight. Membranes were then washed with PBS + 0.1% (v/v) Tween-20, then stained with HRP-conjugated secondary antibodies for 1 h at room temperature. Membranes were washed with PBS + 0.1% (v/v) Tween-20 to remove excess antibody, and reactive bands were visualized using Pierce ECL Western Blotting Substrate (Thermo Scientific #32109) or Super-Signal West Femto Maximum Sensitivity Substrate (Thermo Scientific #34096). Western blot images were collected on a BioRad ChemiDoc XRS+ using the Image Lab software (BioRad).

Antibodies

For immunoblotting experiments, we used anti-METTL3 rabbit polyclonal antibody (Protein-Tech #15073-1-AP) directed against amino acids 229–580 in METTL3, anti-METTL3 rabbit monoclonal antibody (Cell Signalling Technology #96391S) directed against residues surrounding Leu297 of METTL3, and anti-GAPDH rabbit monoclonal antibody (Abcam ab181603) as primary antibodies. All primary antibodies were diluted 1:1,000 in 5% bovine serum albumin in PBS + 0.1% (v/v) Tween-20. Amersham ECL Rabbit IgG, HRP-linked whole antibody from donkey (Cytiva NA934) was used as secondary antibody, at 1:5,000 dilution in 5% bovine serum albumin in PBS + 0.1% (v/v) Tween-20.

5' RACE

5' RACE was performed using the Template Switching RT Enzyme Mix (New England Biolabs M0466) according to manufacturer's instruction, and 1 μ g total RNA was incubated with 10 mM dNTP and 10 mM dT(40) primer at 75°C for 5 min to allow the primer to hybridize. Full-length cDNA was reverse transcribed in 1 \times template switching RT buffer, 1 \times template switching RT enzyme, with 3.75 μ M template switching oligo (GCT AAT CAT TGC AAG GAT CCG TAT CAA CGC AGA GTA CAT rGrGrG) for 90 min at 42°C. RNA was degraded using

5 units RNase H (New England Biolabs M0297) for 30 min. Approximately 10% of the cDNA product was amplified via PCR using a forward primer against the template switching oligo (CAT TGC AAG GAT CCG TAT CAA C, underlined = BamHI cut site) and a reverse primer against *Mettl3* exon 6 (CCA GGT AGC GGA TAT CAC AAC, underlined = EcoRV cut site). PCR amplification was performed in 20 μ l 1 \times Phusion High-Fidelity PCR Master Mix with HF Buffer (NEB M0531) and using touchdown PCR cycling at 98°C for 30 s; 5 cycles of 98°C for 10 s, 72°C for 60 s; 5 cycles of 98°C for 10 s, 70°C for 60 s; 27 cycles of 98°C for 10 s, 65°C for 30 s, 72°C for 60 s; 72°C for 10 min; 4°C hold.

The 5' RACE PCR product was digested using BamHI (New England Biolabs R0136) and EcoRV (New England Biolabs R3195) cut sites found in the primers and cloned into a pcDNA3.1(+) backbone using the Quick Ligation Kit (New England Biolabs M2200). Plasmids were transformed and grown in subcloning efficiency DH5 α competent cells (Invitrogen #18265017) before extraction by Miniprep (QIAGEN #27104) and Sanger sequencing. Sequences of the 5' RACE products can be found in [S1 Table](#).

Cloning and transfection of METTL3 isoform ORFs

ORFs of METTL3 isoforms were identified from the *Mettl3* mRNAs by finding the longest ORF that encoded an AUG start codon, a protein which aligned with the METTL3 protein, and which was not interrupted by premature stop codons. The full sequence of the METTL3 isoform ORFs identified can be found in [S2 Table](#).

The ORFs for full-length METTL3, METTL3-a.i, and METTL3-b.i were constructed via PCR from WT *Mettl3* cDNA. FLAG-tags were included at the N-terminus. Primers used for PCR of the METTL3 isoform ORFs can be found in [S5 Table](#). PCR amplification was performed in 1 \times Phusion High-Fidelity PCR Master Mix with HF Buffer (New England Biolabs M0531) and PCR cycling at 98°C for 30 s; 25 cycles of 98°C for 10 s, 65°C for 30 s, 72°C for 90 s; 72°C for 10 min; 4°C hold. The ORFs were then digested using HindIII (New England Biolabs R0104) and BamHI (New England Biolabs R0136), and cloned into a pcDNA3.1(+) vector using the Quick Ligation Kit (New England Biolabs M2200). All constructs were verified to be identical to the *Mettl3* mRNAs from exon2 *Mettl3* KO mESCs via Sanger sequencing.

Exon-skipping ORFs METTL3-a.ii and METTL3-b.ii were constructed via PCR from WT *Mettl3* cDNA, followed by assembly and cloning into a pcDNA3.1(+) backbone using Gibson Assembly (New England Biolabs E2611). FLAG-tags were included at the N-terminus. Primers used for PCR of the METTL3 isoform ORFs can be found in [S5 Table](#). PCR amplification was performed in 1 \times Phusion High-Fidelity PCR Master Mix with HF Buffer (NEB M0531) and PCR cycling at 98°C for 30 s; 25 cycles of 98°C for 10 s, 65°C for 30 s, 72°C for 90 s; 72°C for 10 min; 4°C hold. Gibson assembly was performed in 1 \times Gibson Assembly Master Mix (New England Biolabs E2611) for 1 h at 50°C with 1:5 ratio of vector to inserts. All constructs were verified to be identical to the *Mettl3* mRNAs from exon2 *Mettl3* KO mESCs via Sanger sequencing.

Plasmids were transformed and grown in high efficiency DH5 α competent cells (New England Biolabs C2987) before extraction by Miniprep (QIAGEN #27104). Sequences were confirmed via Sanger sequencing.

Plasmids were transfected into mESCs using FuGENE HD transfection reagent (Promega E2311). Exon4 WT mESCs or *Mettl3* KO mESCs were plated at 150,000 cells/well on gelatinized (0.1% gelatin in water, EmbryoMax ES-006-B) 6-well plates. The next day, when the mESCs were at 50% confluency, cells were transfected with 2.5 μ g of METTL3 isoform ORF-expressing plasmids using 7.5 μ l FuGene HD reagent per well. After 48 h of transfection, cell lysate was collected for western blot, and RNA was extracted for m⁶A measurements.

Successful transfection was confirmed via western blot using anti-FLAG antibody and anti-METTL3 antibody.

Polysome profiling of *Mettl3* KO cells

Polysomes were isolated from exon2 *Mettl3* KO mESCs as follows: cells were lysed in lysis buffer (20 mM Tris-HCL (pH 7.4), 100 mM KCl, 5 mM MgCl₂, 1% Triton-X 100, 100 µg/ml cycloheximide, 2 mM DTT, 1× Halt Protease Inhibitor (Thermo Scientific #78430)) by passing through a 25 G 1 ½ syringe 10 times. A total of 130 µg of RNA was used per sample. Polysomes were separated using a 10% to 50% sucrose gradient and collected using the Piston Gradient Fractionator (BioComp). Fractions were pooled together as described in S3 Fig, and RNA was extracted using TRIzol LS (Invitrogen #10296010) with 10 mM EDTA to disassemble polysomes.

To identify *Mettl3* mRNAs in the polysome fractions, RNA from each fraction was reverse transcribed using SuperScriptIV (Invitrogen #18090010) and a primer against the most 3' end of the *Mettl3* transcript (S5 Table). PCR amplification was performed using primers against the most 5' end and the most 3' end of the *Mettl3* transcript (S5 Table) in 1× Phusion High-Fidelity PCR Master Mix with HF Buffer (New England Biolabs M0531) and PCR cycling at 98°C for 30 s; 30 cycles of 98°C for 10 s, 65°C for 30 s, 72°C for 90 s; 72°C for 10 min; 4°C hold. PCR products were digested using BamHI (New England Biolabs R0136) and HindIII (New England Biolabs R0104) cut sites found in the primers and cloned into a pcDNA3.1(+) backbone using the Quick Ligation Kit (New England Biolabs M2200). Plasmids were transformed and grown in subcloning efficiency DH5α competent cells (Invitrogen #18265017) before extraction by Miniprep (QIAGEN #27104) and Sanger sequencing.

STM2457 inhibition of METTL3

Cells were seeded to be 50% confluent. The next day, cells were treated with 30 µM STM2457 or with equal volume DMSO (negative control). After 48 h of treatment, total RNA was extracted from cells using TRIzol Reagent (Invitrogen #15596026) for m⁶A measurements.

2D-TLC measurement of m⁶A

m⁶A levels in mRNA were measured by 2D-TLC (2-dimensional thin-layer chromatography) as described previously [77]. m⁶A was poly-A selected twice using Dynabeads Oligo(dT)₂₅ (Invitrogen #61002) according to manufacturer's protocol to remove potential contamination from ribosomal RNAs or other noncoding RNAs. A total of 100 ng of twice poly-A-selected RNA was then digested by 1 U RNase T1 (Invitrogen AM2283) in 1× PNK buffer for 2 h at 37°C. This cuts mRNA after G, therefore only exposing m⁶As in a GA context and omitting m⁶As in the poly-A tail or in other non-mRNA contexts. The 5' end of the digested RNA is then labeled with 10 U T4 PNK (New England Biolabs M0201) and 10 µCi [γ-³²P]ATP (Perkin Elmer BLU002Z250UC) for 30 min at 37°C; γ-phosphate was then removed from excess [γ-³²P]ATP with 0.5 U apyrase (New England Biolabs M0398) in 1× apyrase buffer for 10 min at 30°C. RNA was then digested to single nucleotides using 2 U Nuclease P1 (FUJIFILM Wako Pure Chemical Corporation #145-08221) for 1 h at 60°C.

2 µl of the digested RNA is spotted on PEI-cellulose TLC plates (Millipore Sigma #105579) 0.5 µl at a time. Plates were developed in 5:3 (v/v) isobutyric acid:0.5 M NH₄OH in the first dimension, then in 70:15:15 (v/v/v) isopropanol:water:HCl in the second dimension. Radioactively labeled nucleotides were detected using a phosphor storage screen and Amersham Biosciences Typhoon 9400 Variable Mode Imager. m⁶A levels were quantified using Image Lab software (BioRad).

DepMap dataset analysis

Gene dependency probability scores were obtained from the DepMap Public 21Q4 CRISPR gene dependency dataset [43–47]. We extracted the gene dependency probability scores of 1,054 cell lines on the gene *METTL3* and plotted them to identify cell lines that were dependent on *METTL3*. Gene dependency probability scores greater than 0.5 indicate that a cell line is dependent on the gene. To account for off-target effects, we extracted the gene dependency scores of 1,054 cell lines on *METTL3*, *METTL14*, and *WTAP*. We identified cell lines that were dependent on all of these genes (gene dependency probability scores >0.5).

To identify cell lines that may be independent of m⁶A, we extracted the gene dependency scores of 1,054 cell lines on *METTL3*, *METTL14*, and *WTAP*. We identified cell lines that were independent of each of these genes (gene dependency probability scores <0.5). We next identified cell lines that were independent of all 3 genes to obtain a subset of cell lines that may be independent of m⁶A. The full list of predicted m⁶A-independent cell lines can be found in [S4 Table](#).

Generation of *Mettl3* conditional KO MEFs

Mettl3^{lox/lox} mice were generated based on construction from the Knockout Mouse Project Repository (KOMP) and were described by Cheng and colleagues [32]. *loxP* sites were inserted spanning the fourth exon of *Mettl3*.

To generate tamoxifen-inducible *Mettl3* KO MEFs, embryos from *Mettl3^{lox/lox}* mice were collected on day 13.5, mechanically separated, trypsinized, and plated. After 3 passages, cells were transduced with SV40 large T-antigen and passaged until they reached senescence. Cells that escaped senescence and became immortalized were then infected with Cre-ERT2 lentivirus. Successfully infected cells were selected with puromycin. Single-cell colonies were then isolated and expanded.

To induce the *Mettl3* knockout, MEFs were plated at 100,000 cells/well in a 12-well plate. The next day, when the MEFs were at 50% confluency, cells were treated with 4-hydroxytamoxifen (500 nM) or ethanol (negative control) for 48 h. Cells continued to be grown and passaged normally after 4-hydroxytamoxifen treatment. Cell lysate was collected 5 days after tamoxifen treatment for western blot. RNA was collected 8 days after tamoxifen treatment for m⁶A measurements.

MTT assay

To measure the changes in cell proliferation upon *Mettl3* KO, tamoxifen-inducible *Mettl3* KO MEFs were plated at 5,000 cells/well in a 12-well plate. The next day, cells were treated with 4-hydroxytamoxifen (500 nM) or ethanol (negative control). Treatment continued for the duration of the experiment, and then, 0, 2, 4, 6, and 8 days after 4-hydroxytamoxifen treatment, cells were washed with PBS and then incubated in 1:1 (v/v) high-glucose DMEM without phenol red (Gibco #21063029) and MTT (3-(4,5-dimethylthiazol-2-yl)-2,5-diphenyltetrazolium bromide) reagent (5 mg/ml MTT (Abcam ab146345) in PBS) for 3 h at 37°C. The produced formazan crystals were dissolved in 1.5× volume MTT solvent (4 mM HCl, 0.1% NP-40 in isopropanol) and incubated for 15 min at room temperature while shaking on an orbital shaker. Samples without cells were included as background controls. Absorbance was read at 570 nM to estimate the number of cells.

Supporting information

S1 Fig. Exon2 *Mettl3* KO mESCs express altered METTL3 proteins while exon4 *Mettl3* KO mESCs do not. (A) Exon2 *Mettl3* KO mESCs express a novel protein that is immunoreactive to several anti-METTL3 antibodies. We found that exon2 *Mettl3* KO mESCs express new proteins that are reactive to an anti-METTL3 pAb. To confirm that these new proteins may be shortened versions of METTL3, we performed a second WB with a different anti-METTL3 mAb. Similar to the first WB, we found that full-length METTL3 (75 kDa, arrowhead) was lost in both KO cell lines. In the KO cell lines, the same bands that were immunoreactive to the polyclonal anti-METTL3 antibody were also immunoreactive to the anti-METTL3 mAb at approximately 50 kDa in *Mettl3* KO mESC-a and approximately 55 kDa in *Mettl3* KO mESC-b, respectively (arrowheads). This further validates the possibility that the *Mettl3* KO mESCs express smaller versions of METTL3 proteins. 30 μ g per lane. (B) Exon4 *Mettl3* KO mESCs do not express METTL3 protein. An independently run replicate of the WB from Fig 1B reveals that exon4 *Mettl3* KO mESCs do not express any proteins immunoreactive to anti-METTL3 antibodies. 30 μ g per lane. (C) Exon4 *Mettl3* KO mESCs do not express METTL3 protein. To confirm that exon4 *Mettl3* KO mESCs do not express METTL3, we performed a second WB with a different anti-METTL3 mAb. We confirmed that exon4 *Mettl3* KO mESCs indeed do not express any detectable METTL3 protein. 30 μ g per lane. mAb, monoclonal antibody; mESC, mouse embryonic stem cell; pAb, polyclonal antibody; WB, western blot; WT, wild-type. (TIFF)

S2 Fig. Mouse embryonic stem cells are transfected at low efficiency. Transfection efficiency of mESCs is low. Optimization of transfection conditions using plasmids expressing eGFP showed that only 10% to 30% of mESCs become successfully transfected and express eGFP after 48 h. This suggests that only a small number of cells will express proteins after plasmid transfection, and may explain the low level of m⁶A rescue after transfection of exon4 *Mettl3* KO mESCs with WT METTL3 (Fig 2C). eGFP, enhanced green fluorescent protein; mESC, mouse embryonic stem cell; WT, wild-type. (TIFF)

S3 Fig. Polysome profiling reveals that exon2 *Mettl3* KO mESCs translate *Mettl3* mRNAs. To investigate if the altered *Mettl3* mRNAs expressed in the exon2 *Mettl3* KO mESCs are translated, we performed polysome profiling. The polysomes were separated into 4 fractions based on their ribosome load: Fraction 1 (sub-monosomal), Fraction 2 (low polysomes), Fraction 3 (medium polysomes), and Fraction 4 (high polysomes). RT-PCR of *Mettl3* using primers against the 5' and 3' end of *Mettl3* revealed *Mettl3* mRNAs (arrowheads) in the medium and high polysome fractions in the WT mESCs, as well as the exon2 *Mettl3* KO mESCs. Sequencing of the PCR products revealed *Mettl3* mRNAs depicted in blue. They include *mRNA-3* that encodes METTL3-a.ii in exon2 *Mettl3* KO mESC-a, and *mRNA-7* that encodes METTL3-b.ii in exon 2 *Mettl3* KO mESC-b (S3 Table). This suggests that the *Mettl3* mRNAs being expressed can indeed be translated to produce the METTL3 proteins we see in these *Mettl3* KO cell lines. Underlying data can be found in S1 Data. mESC, mouse embryonic stem cell; RT-PCR, reverse transcription PCR; WT, wild-type. (TIFF)

S4 Fig. STM2457 treatment has no effect on m⁶A in exon4 *Mettl3* KO mESCs. Treatment of exon4 *Mettl3* KO mESCs with the METTL3-specific inhibitor STM2457 does not reduce m⁶A levels. Treatment of the parental WT mESC cell line with 30 μ M of STM2457 lead to 65.4% reduction in m⁶A levels. On the other hand, STM2457 treatment did not lead to a significant

change in m⁶A levels in exon4 *Mettl3* KO mESCs, indicating that the small amount of remaining m⁶A was not produced by METTL3. Error bars indicate standard error ($n = 3$). * = p -value < 0.5, ** = p -value < 0.01, *** = p -value < 0.005, n.s. = not significant. Underlying data can be found in [S1 Data](#). m⁶A, N⁶-methyladenosine; m⁷GMP, 7-methylguanosine monophosphate; mESC, mouse embryonic stem cell; WT, wild-type.

(TIFF)

S5 Fig. *METTL3* KO A549 cells have high m⁶A levels. (A) *METTL3* KO A549 cells have persistent m⁶A. *METTL3* KO A549 cells were previously reported [38]. To find out how much m⁶A remains in these cells, we measured the levels of m⁶A using 2D-TLC that measures m⁶A specifically in the GA context [77]. This limits the detection of m⁶A to only m⁶A in mRNAs, where they are found in a DRACH context [58,71,72]. The m⁶A level in the *METTL3* KO A549 cells was very similar to m⁶A levels in WT A549 cells. This suggests that either the knock-out of *METTL3* was incomplete or that A549 cells may express a non-*METTL3* m⁶A methyltransferase that is responsible for the majority of m⁶A in mRNAs ($n = 1$). Underlying data can be found in [S1 Data](#). 2D-TLC, 2-dimensional thin-layer chromatography; m⁶A, N⁶-methyladenosine; WT, wild-type.

(TIFF)

S6 Fig. A large number of cell lines are dependent on the m⁶A methyltransferase complex components *METTL3*, *METTL14*, and *WTAP*. A large number of cell lines are dependent on the components of the m⁶A methyltransferase complex for proliferation. Using the DepMap CRISPR loss-of-function screening dataset, we found that 801 of 1,054 tested cell lines require *METTL3* for proliferation (Fig 4A). In order to assess the influence of off-target effects on this result, we further analyzed the dataset to find cell lines that are dependent on other members of the m⁶A methyltransferase complex, *WTAP*, and *METTL14*. We find that 683 of the 801 *METTL3*-dependent cell lines are also dependent on both *METTL14* and *WTAP*. The large overlap in cell lines dependent on the m⁶A methyltransferase complex members suggests that these cell lines are truly dependent on m⁶A methyltransferase activity, and the contribution of off-target effects in the CRISPR screen for *METTL3* dependence is low. m⁶A, N⁶-methyladenosine.

(TIFF)

S7 Fig. Depletion of *METTL3* leads to slower proliferation in MEFs. (A) *Mettl3* conditional knockout MEFs do not express METTL3 protein. To confirm that *Mettl3* is the sole m⁶A writer in cell lines other than mESCs, we produced a tamoxifen-inducible *Mettl3* conditional knockout MEF cell line. We used a WB to confirm the loss of METTL3 using a second anti-METTL3 mAb. Five days after 4OHT treatment (500 nM), we observe loss of the WT METTL3 protein. 30 μ g per lane. (B) *Mettl3* knockout in MEFs leads to a decrease in cellular proliferation. Using an MTT assay, we measured cell proliferation after 4OHT-induced *METTL3* knockout over 8 days. Proliferation of *Mettl3* KO MEFs began to slow down compared to WT MEFs after 6 days of 4OHT treatment. Error bars indicate standard error ($n = 3$). * = p -value < 0.5, ** = p -value < 0.01, *** = p -value < 0.005, n.s. = not significant. Underlying data can be found in [S1 Data](#). mAb, monoclonal antibody; m⁶A, N⁶-methyladenosine; MEF, mouse embryonic fibroblast; mESC, mouse embryonic stem cell; WB, western blot; 4OHT, 4-hydroxytamoxifen.

(TIFF)

S1 Table. Sequences of 5' RACE products from *Mettl3* in exon2 *Mettl3* KO mESCs. mESC, mouse embryonic stem cell; RACE, rapid amplification of cDNA ends.

(XLSX)

S2 Table. Sequences of METTL3 ORFs identified in exon2 *Mettl3* KO mESCs. mESC, mouse embryonic stem cell; ORF, open reading frame.

(XLSX)

S3 Table. Sequences of *Mettl3* mRNAs identified in polysome fractions.

(XLSX)

S4 Table. List of cell lines predicted to be m⁶A-independent. m⁶A, N⁶-methyladenosine.

(CSV)

S5 Table. Primers used in this manuscript.

(XLSX)

S1 Data. Underlying data for figures in this manuscript.

(XLSX)

S1 Raw images. Raw images for all gels and Western blots in this manuscript.

(PDF)

Acknowledgments

We thank members of the Jaffrey Lab for helpful comments and suggestions.

Author Contributions

Conceptualization: Hui Xian Poh, Samie R. Jaffrey.

Investigation: Hui Xian Poh, Aashiq H. Mirza, Brian F. Pickering.

Methodology: Hui Xian Poh, Aashiq H. Mirza, Brian F. Pickering.

Validation: Hui Xian Poh.

Visualization: Hui Xian Poh.

Writing – original draft: Hui Xian Poh, Samie R. Jaffrey.

References

1. Perry RP, Kelley DE. Existence of methylated messenger RNA in mouse L cells. *Cell*. 1974; 1:37–42. [https://doi.org/10.1016/0092-8674\(74\)90153-6](https://doi.org/10.1016/0092-8674(74)90153-6)
2. Desrosiers R, Friderici K, Rottman F. Identification of methylated nucleosides in messenger RNA from Novikoff hepatoma cells. *Proc Natl Acad Sci U S A*. 1974; 71:3971–5. <https://doi.org/10.1073/pnas.71.10.3971> PMID: 4372599
3. Meyer KD, Saletore Y, Zumbo P, Elemento O, Mason CE, Jaffrey SR, et al. Comprehensive analysis of mRNA methylation reveals enrichment in 3' UTRs and near stop codons. *Cell*. 2012; 149:1635–46. <https://doi.org/10.1016/j.cell.2012.05.003> PMID: 22608085
4. Batista PJ, Molinie B, Wang J, Qu K, Zhang J, Li L, et al. m⁶A RNA modification controls cell fate transition in mammalian embryonic stem cells. *Cell Stem Cell*. 2014; 15:707–19. <https://doi.org/10.1016/j.stem.2014.09.019> PMID: 25456834
5. Geula S, Moshitch-Moshkovitz S, Dominissini D, Mansour AAF, Kol N, Salmon-Divon M, et al. m⁶A mRNA methylation facilitates resolution of naïve pluripotency toward differentiation. *Science*. 2015; 347:1002–6. <https://doi.org/10.1126/science.1261417> PMID: 25569111
6. Wang Y, Li Y, Toth JI, Petroski MD, Zhang Z, Zhao JC. N⁶-methyladenosine modification destabilizes developmental regulators in embryonic stem cells. *Nat Cell Biol*. 2014; 16:191–8. <https://doi.org/10.1038/ncb2902> PMID: 24394384
7. Barbieri I, Tzelepis K, Pandolfini L, Shi J, Millán-Zambrano G, Robson SC, et al. Promoter-bound METTL3 maintains myeloid leukaemia by m⁶A-dependent translation control. *Nature*. 2017; 552:126–31. <https://doi.org/10.1038/nature24678> PMID: 29186125

8. Vu LP, Pickering BF, Cheng Y, Zaccara S, Nguyen D, Minuesa G, et al. The N^6 -methyladenosine (m^6A)-forming enzyme METTL3 controls myeloid differentiation of normal hematopoietic and leukemia cells. *Nat Med*. 2017; 23:1369–76. <https://doi.org/10.1038/nm.4416> PMID: 28920958
9. Dixit D, Xie Q, Rich JN, Zhao JC. Messenger RNA methylation regulates glioblastoma tumorigenesis. *Cancer Cell*. 2017; 31(4):474–5. <https://doi.org/10.1016/j.ccell.2017.03.010> PMID: 28399407
10. Zhao BS, Wang X, Beadell A, Lu Z, Shi H, Kuuspalu A, et al. m^6A -dependent maternal mRNA clearance facilitates zebrafish maternal-to-zygotic transition. *Nature*. 2017; 542:475–8. <https://doi.org/10.1038/nature21355> PMID: 28192787
11. Fustin JM, Doi M, Yamaguchi Y, Hida H, Nishimura S, Yoshida M, et al. RNA-methylation-dependent RNA processing controls the speed of the circadian clock. *Cell*. 2013; 155:793. <https://doi.org/10.1016/j.cell.2013.10.026> PMID: 24209618
12. Zhou J, Wan J, Gao X, Zhang X, Jaffrey SR, Qian SB. Dynamic m^6A mRNA methylation directs translational control of heat shock response. *Nature*. 2015; 526:591–4. <https://doi.org/10.1038/nature15377> PMID: 26458103
13. Merkestein M, Laber S, McMurray F, Andrew D, Sachse G, Sanderson J, et al. FTO influences adipogenesis by regulating mitotic clonal expansion. *Nat Commun*. 2015; 6:6792. <https://doi.org/10.1038/ncomms7792> PMID: 25881961
14. Zhao X, Yang Y, Sun BF, Shi Y, Yang X, Xiao W, et al. FTO-dependent demethylation of N^6 -methyladenosine regulates mRNA splicing and is required for adipogenesis. *Cell Res*. 2014; 24:1403–19. <https://doi.org/10.1038/cr.2014.151> PMID: 25412662
15. Roundtree IA, Evans ME, Pan T, He C. Dynamic RNA modifications in gene expression regulation. *Cell*. 2017; 169(7):1187–200. <https://doi.org/10.1016/j.cell.2017.05.045> PMID: 28622506
16. Zhao BS, Roundtree IA, He C. Post-transcriptional gene regulation by mRNA modifications. *Nat Rev Mol Cell Biol*. 2016; 18:31–42. <https://doi.org/10.1038/nrm.2016.132> PMID: 27808276
17. Zaccara S, Ries RJ, Jaffrey SR. Reading, writing and erasing mRNA methylation. *Nat Rev Mol Cell Biol*. 2019; 20:608–24. <https://doi.org/10.1038/s41580-019-0168-5> PMID: 31520073
18. Bokar JA, Shambaugh ME, Polayes D, Matera AG, Rottman FM. Purification and cDNA cloning of the AdoMet-binding subunit of the human mRNA (N^6 -adenosine)-methyltransferase. *RNA*. 1997; 3:1233–47. Available from: <https://rnajournal.cshlp.org/content/3/11/1233>. PMID: 9409616
19. Wang P, Doxtader KA, Nam Y. Structural Basis for cooperative function of Mettl3 and Mettl14 methyltransferases. *Mol Cell*. 2016; 63:306–17. <https://doi.org/10.1016/j.molcel.2016.05.041> PMID: 27373337
20. Wang X, Feng J, Xue Y, Guan Z, Zhang D, Liu Z, et al. Structural basis of N^6 -adenosine methylation by the METTL3-METTL14 complex. *Nature*. 2016; 534:575–8. <https://doi.org/10.1038/nature18298> PMID: 27281194
21. Liu J, Yue Y, Han D, Wang X, Fu Y, Zhang L, et al. A METTL3-METTL14 complex mediates mammalian nuclear RNA N^6 -adenosine methylation. *Nat Chem Biol*. 2014; 10:93–5. <https://doi.org/10.1038/nchembio.1432> PMID: 24316715
22. Schwartz S, Mumbach MR, Jovanovic M, Wang T, Maciag K, Bushkin GG, et al. Perturbation of m^6A writers reveals two distinct classes of mRNA methylation at internal and 5' sites. *Cell Rep*. 2014; 8:284–96. <https://doi.org/10.1016/j.celrep.2014.05.048> PMID: 24981863
23. Xiang Y, Laurent B, Hsu CH, Nachtergaele S, Lu Z, Sheng W, et al. RNA m^6A methylation regulates the ultraviolet-induced DNA damage response. *Nature*. 2017; 543:573–6. <https://doi.org/10.1038/nature21671> PMID: 28297716
24. Fu Y, Zhuang X. m^6A -binding YTHDF proteins promote stress granule formation. *Nat Chem Biol*. 2020; 16:955–63. <https://doi.org/10.1038/s41589-020-0524-y> PMID: 32451507
25. Zhang H, Shi X, Huang T, Zhao X, Chen W, Gu N, et al. Dynamic landscape and evolution of m^6A methylation in human. *Nucleic Acids Res*. 2020; 48:6251–64. <https://doi.org/10.1093/nar/gkaa347> PMID: 32406913
26. Jiang L, Chen T, Xiong L, Xu JH, Gong AY, Dai B, et al. Knockdown of m^6A methyltransferase METTL3 in gastric cancer cells results in suppression of cell proliferation. *Oncol Lett*. 2020; 20:2191–8. <https://doi.org/10.3892/ol.2020.11794> PMID: 32782536
27. Shen C, Xuan B, Yan T, Ma Y, Xu P, Tian X, et al. m^6A -dependent glycolysis enhances colorectal cancer progression. *Mol Cancer*. 2020; 19:1–19. <https://doi.org/10.1186/s12943-020-01190-w> PMID: 32245489
28. Xu J, Chen Q, Tian K, Liang R, Chen T, Gong A, et al. m^6A methyltransferase METTL3 maintains colon cancer tumorigenicity by suppressing SOCS2 to promote cell proliferation. *Oncol Rep*. 2020; 44:973–86. <https://doi.org/10.3892/or.2020.7665> PMID: 32705223

29. Wu Z, Shi Y, Lu M, Song M, Yu Z, Wang J, et al. METTL3 counteracts premature aging via m⁶A-dependent stabilization of MIS12 mRNA. *Nucleic Acids Res.* 2020; 48:11083–96. <https://doi.org/10.1093/nar/gkaa816> PMID: 33035345
30. Li HB, Tong J, Zhu S, Batista PJ, Duffy EE, Zhao J, et al. m⁶A mRNA methylation controls T cell homeostasis by targeting the IL-7/STAT5/SOCS pathways. *Nature.* 2017; 548:338–42. <https://doi.org/10.1038/nature23450> PMID: 28792938
31. Lin Z, Hsu PJ, Xing X, Fang J, Lu Z, Zou Q, et al. Mettl3-/Mettl14-mediated mRNA N⁶-methyladenosine modulates murine spermatogenesis. *Cell Res.* 2017; 27:1216–30. <https://doi.org/10.1038/cr.2017.117> PMID: 28914256
32. Cheng Y, Luo H, Jaffrey SR, Landau DA, Kharas MG. m⁶A RNA methylation maintains hematopoietic stem cell identity and symmetric commitment. *Cell Rep.* 2019;28. <https://doi.org/10.1016/j.celrep.2019.07.032> PMID: 31412241
33. Tong J, Wang X, Liu Y, Ren X, Wang A, Chen Z, et al. Pooled CRISPR screening identifies m⁶A as a positive regulator of macrophage activation. *Sci Adv.* 2021; 7:eabd4742. <https://doi.org/10.1126/sciadv.abd4742> PMID: 33910903
34. Wei G, Almeida M, Pintacuda G, Coker H, Bowness JS, Ule J, et al. Acute depletion of METTL3 implicates N⁶-methyladenosine in alternative intron/exon inclusion in the nascent transcriptome. *Genome Res.* 2021; 31:1395–408. <https://doi.org/10.1101/gr.271635.120> PMID: 34131006
35. Su R, Dong L, Li Y, Gao M, He PC, Liu W, et al. METTL16 exerts an m⁶A-independent function to facilitate translation and tumorigenesis. *Nat Cell Biol.* 2022; 24:205–16. <https://doi.org/10.1038/s41556-021-00835-2> PMID: 35145225
36. Huang J, Dong X, Gong Z, Qin L-Y, Yang S, Zhu Y-L, et al. Solution structure of the RNA recognition domain of METTL3-METTL14 N⁶-methyladenosine methyltransferase. *Protein Cell.* 2019; 10:272–84. <https://doi.org/10.1007/s13238-018-0518-7> PMID: 29542011
37. Mirza AH, Attarwala N, Gross S, Chen Q, Jaffrey SR. Selective detection of m⁶A derived from mRNA using the Phospho-tag m⁶A assay. *bioRxiv.* 2022; 2022.05.23.493172. <https://doi.org/10.1101/2022.05.23.493172>
38. Schramm G, Bruchhaus I, Roeder T. A simple and reliable 5'-RACE approach. *Nucleic Acids Res.* 2000; 28:96. <https://doi.org/10.1093/nar/28.22.e96> PMID: 11071950
39. Schöller E, Weichmann F, Treiber T, Ringle S, Treiber N, Flatley A, et al. Interactions, localization, and phosphorylation of the m⁶A generating METTL3–METTL14–WTAP complex. *RNA.* 2018; 24:499–512. <https://doi.org/10.1261/rna.064063.117> PMID: 29348140
40. Yankova E, Blackaby W, Albertella M, Rak J, de Braekeleer E, Tsagkogeorga G, et al. Small-molecule inhibition of METTL3 as a strategy against myeloid leukaemia. *Nature.* 2021; 593:597–601. <https://doi.org/10.1038/s41586-021-03536-w> PMID: 33902106
41. Courtney DG, Kennedy EM, Dumm RE, Bogerd HP, Tsai K, Heaton NS, et al. Epitranscriptomic enhancement of influenza A virus gene expression and replication. *Cell Host Microbe.* 2017; 22:377–386.e5. <https://doi.org/10.1016/j.chom.2017.08.004> PMID: 28910636
42. Chen H, Gao S, Liu W, Wong CC, Wu J, Wu J, et al. RNA N⁶-methyladenosine methyltransferase mettl3 facilitates colorectal cancer by activating the m⁶A-GLUT1-mTORC1 axis and is a therapeutic target. *Gastroenterology.* 2021; 160:1284–1300.e16. <https://doi.org/10.1053/j.gastro.2020.11.013> PMID: 33217448
43. Meyers RM, Bryan JG, McFarland JM, Weir BA, Sizemore AE, Xu H, et al. Computational correction of copy number effect improves specificity of CRISPR-Cas9 essentiality screens in cancer cells. *Nat Genet.* 2017; 49:1779–84. <https://doi.org/10.1038/ng.3984> PMID: 29083409
44. Dempster J, Rossen J, Kazachkova M, Pan J, Kugener G, Root D, et al. Extracting biological insights from the project Achilles genome-scale CRISPR screens in cancer cell lines. *bioRxiv.* 2019:720243. <https://doi.org/10.1101/720243>
45. Pacini C, Dempster JM, Boyle I, Gonçalves E, Najgebauer H, Karakoc E, et al. Integrated cross-study datasets of genetic dependencies in cancer. *Nat Commun.* 2021; 12:1–14.
46. Dempster JM, Boyle I, Vazquez F, Root D, Boehm JS, Hahn WC, et al. Chronos: a CRISPR cell population dynamics model. *bioRxiv.* 2021; 2021.02.25.432728. <https://doi.org/10.1038/s41419-020-03071-y> PMID: 34930405
47. DepMap, Broad. DepMap 21Q4 Public. In: figshare [Internet]. 2021 [cited 2021 Nov 15]. https://figshare.com/articles/dataset/DepMap_21Q4_Public/16924132/1.
48. Ping XL, Sun BF, Wang L, Xiao W, Yang X, Wang WJ, et al. Mammalian WTAP is a regulatory subunit of the RNA N⁶-methyladenosine methyltransferase. *Cell Res.* 2014; 24:177–89. <https://doi.org/10.1038/cr.2014.3> PMID: 24407421

49. Wang Q, Guo X, Li L, Gao Z, Su X, Ji M, et al. *N*⁶-methyladenosine METTL3 promotes cervical cancer tumorigenesis and Warburg effect through YTHDF1/HK2 modification. *Cell Death Dis.* 2020; 11:1–10. <https://doi.org/10.1038/s41419-019-2182-0> PMID: 31911576
50. Wang H, Xu B, Shi J. *N*⁶-methyladenosine METTL3 promotes the breast cancer progression via targeting Bcl-2. *Gene.* 2020; 722:144076. <https://doi.org/10.1016/j.gene.2019.144076> PMID: 31454538
51. Yue B, Song C, Yang L, Cui R, Cheng X, Zhang Z, et al. METTL3-mediated *N*⁶-methyladenosine modification is critical for epithelial-mesenchymal transition and metastasis of gastric cancer. *Mol Cancer.* 2019; 18:1–15. <https://doi.org/10.1186/s12943-019-1065-4> PMID: 30609930
52. Visvanathan A, Patil V, Abdulla S, Hoheisel JD, Somasundaram K. *N*⁶-methyladenosine landscape of glioma stem-like cells: METTL3 is essential for the expression of actively transcribed genes and sustenance of the oncogenic signaling. *Genes.* 2019; 10(2):141. <https://doi.org/10.3390/genes10020141> PMID: 30781903
53. Jinek M, Chylinski K, Fonfara I, Hauer M, Doudna JA, Charpentier E. A programmable dual-RNA-guided DNA endonuclease in adaptive bacterial immunity. *Science.* 2012; 337:816–21. <https://doi.org/10.1126/science.1225829> PMID: 22745249
54. Ran FA, Hsu PD, Wright J, Agarwala V, Scott DA, Zhang F. Genome engineering using the CRISPR-Cas9 system. *Nat Protoc.* 2013; 8:2281–308. <https://doi.org/10.1038/nprot.2013.143> PMID: 24157548
55. Kapahnke M, Banning A, Tikkanen R. Random splicing of several exons caused by a single base change in the target exon of CRISPR/Cas9 mediated gene knockout. *Cell.* 2016; 5:45. <https://doi.org/10.3390/cells5040045> PMID: 27983621
56. Mou H, Smith JL, Peng L, Yin H, Moore J, Zhang XO, et al. CRISPR/Cas9-mediated genome editing induces exon skipping by alternative splicing or exon deletion. *Genome Biol.* 2017; 18:1–8.
57. Lalonde S, Stone OA, Lessard S, Lavertu A, Desjardins J, Beaudoin M, et al. Frameshift indels introduced by genome editing can lead to in-frame exon skipping. *PLoS ONE.* 2017; 12:e0178700. <https://doi.org/10.1371/journal.pone.0178700> PMID: 28570605
58. Schulz TJ, Glaubitz M, Kuhlow D, Thierbach R, Birringer M, Steinberg P, et al. Variable expression of Cre recombinase transgenes precludes reliable prediction of tissue-specific gene disruption by tail-biopsy genotyping. *PLoS ONE.* 2007; 2:e1013. <https://doi.org/10.1371/journal.pone.0001013> PMID: 17925861
59. Dominissini D, Moshitch-Moshkovitz S, Schwartz S, Salmon-Divon M, Ungar L, Osenberg S, et al. Topology of the human and mouse m⁶A RNA methylomes revealed by m⁶A-seq. *Nature.* 2012; 485:201–6. <https://doi.org/10.1038/nature11112> PMID: 22575960
60. Linder B, Grozhik AV, Olarerin-George AO, Meydan C, Mason CE, Jaffrey SR. Single-nucleotide-resolution mapping of m⁶A and m⁶Am throughout the transcriptome. *Nat Methods.* 2015; 12:767–72. <https://doi.org/10.1038/nmeth.3453> PMID: 26121403
61. Koh CWQ, Goh YT, Goh WSS. Atlas of quantitative single-base-resolution *N*⁶-methyl-adenine methylomes. *Nat Commun.* 2019; 10:1–15. <https://doi.org/10.1038/s41467-019-13561-z> PMID: 30602773
62. Zhang Z, Chen T, Chen HX, Xie YY, Chen LQ, Zhao YL, et al. Systematic calibration of epitranscriptomic maps using a synthetic modification-free RNA library. *Nat Methods.* 2021; 18:1213–22. <https://doi.org/10.1038/s41592-021-01280-7> PMID: 34594034
63. Schwartz S, Agarwala SD, Mumbach MR, Jovanovic M, Mertins P, Shishkin A, et al. High-Resolution mapping reveals a conserved, widespread, dynamic mRNA methylation program in yeast meiosis. *Cell.* 2013; 155:1409–21. <https://doi.org/10.1016/j.cell.2013.10.047> PMID: 24269006
64. Ke S, Pandya-Jones A, Saito Y, Fak JJ, Vågbo CB, Geula S, et al. m⁶A mRNA modifications are deposited in nascent pre-mRNA and are not required for splicing but do specify cytoplasmic turnover. *Genes Dev.* 2017; 31:990–1006. <https://doi.org/10.1101/gad.301036.117> PMID: 28637692
65. McIntyre ABR, Gokhale NS, Cerchiotti L, Jaffrey SR, Horner SM, Mason CE. Limits in the detection of m⁶A changes using MeRIP/m⁶A-seq. *Sci Rep.* 2020; 10:6590. <https://doi.org/10.1038/s41598-020-63355-3> PMID: 32313079
66. Liu N, Parisien M, Dai Q, Zheng G, He C, Pan T. Probing *N*⁶-methyladenosine RNA modification status at single nucleotide resolution in mRNA and long noncoding RNA. *RNA.* 2013; 19:1848–56. <https://doi.org/10.1261/rna.041178.113> PMID: 24141618
67. Warda AS, Kretschmer J, Hackert P, Lenz C, Urlaub H, Höbartner C, et al. Human METTL16 is a *N*⁶-methyladenosine (m⁶A) methyltransferase that targets pre-mRNAs and various non-coding RNAs. *EMBO Rep.* 2017; 18:2004–14. <https://doi.org/10.15252/embr.201744940> PMID: 29051200
68. Pendleton KE, Chen B, Liu K, Hunter OV, Xie Y, Tu BP, et al. The U6 snRNA m⁶A methyltransferase METTL16 regulates SAM synthetase intron retention. *Cell.* 2017; 169:824–835.e14. <https://doi.org/10.1016/j.cell.2017.05.003> PMID: 28525753

69. Epstein P, Reddy R, Henning D, Busch H. The nucleotide sequence of nuclear U6 (4.7 S) RNA. *J Biol Chem.* 1980; 255:8901–6. [https://doi.org/10.1016/s0021-9258\(18\)43587-9](https://doi.org/10.1016/s0021-9258(18)43587-9) PMID: 6773955
70. Harada F, Kato N, Nishimura S. The nucleotide sequence of nuclear 4.8S RNA of mouse cells. *Top Catal.* 1980; 95:1332–40. [https://doi.org/10.1016/0006-291x\(80\)91620-4](https://doi.org/10.1016/0006-291x(80)91620-4) PMID: 6251836
71. Doxtader KA, Wang P, Scarborough AM, Seo D, Conrad NK, Correspondence YN, et al. Structural Basis for Regulation of METTL16, an S-Adenosylmethionine Homeostasis Factor Article Structural Basis for Regulation of METTL16, an S-Adenosylmethionine Homeostasis Factor. *Mol Cell.* 2018;71. <https://doi.org/10.1016/j.molcel.2018.07.025> PMID: 30197297
72. Wei CM, Gershowitz A, Moss B. 5'-Terminal and Internal Methylated Nucleotide Sequences in Hela Cell mRNA. *Biochemistry.* 1976; 15:397–401. <https://doi.org/10.1021/bi00647a024> PMID: 174715
73. Schibler U, Kelley DE, Perry RP. Comparison of methylated sequences in messenger RNA and heterogeneous nuclear RNA from mouse L cells. *J Mol Biol.* 1977; 115:695–714. [https://doi.org/10.1016/0022-2836\(77\)90110-3](https://doi.org/10.1016/0022-2836(77)90110-3) PMID: 592376
74. van Tran N, Ernst FGM, Hawley BR, Zorbas C, Ulryck N, Hackert P, et al. The human 18S rRNA m⁶A methyltransferase METTL5 is stabilized by TRMT112. *Nucleic Acids Res.* 2019; 47:7719–33. <https://doi.org/10.1093/nar/gkz619> PMID: 31328227
75. Ma H, Wang X, Cai J, Dai Q, Natchiar SK, Lv R, et al. N⁶-Methyladenosine methyltransferase ZCCHC4 mediates ribosomal RNA methylation. *Nat Chem Biol.* 2019; 15:88–94. <https://doi.org/10.1038/s41589-018-0184-3> PMID: 30531910
76. Pinto R, Vågbo CB, Jakobsson ME, Kim Y, Baltissen MP, O'Donohue MF, et al. The human methyltransferase ZCCHC4 catalyses N⁶-methyladenosine modification of 28S ribosomal RNA. *Nucleic Acids Res.* 2020; 48:830–46. <https://doi.org/10.1093/nar/gkz1147> PMID: 31799605
77. Zhong S, Li H, Bodi Z, Button J, Vespa L, Herzog M, et al. MTA is an *Arabidopsis* messenger RNA adenosine methylase and interacts with a homolog of a sex-specific splicing factor. *Plant Cell.* 2008; 20:1278–88. <https://doi.org/10.1105/tpc.108.058883> PMID: 18505803